Supporting Information

Exchange Coupling Mediated Through-Bonds and Through-Space in Conformationally-Constrained Polyradical Scaffolds: Calix[4]arene Nitroxide Tetraradicals And Diradical.

Andrzej Rajca,[a] Sumit Mukherjee,[a] Maren Pink,[b] Suchada Rajca[a]*

Department of Chemistry, University of Nebraska, Lincoln, NE 68588-0304. IUMSC, Department of Chemistry, Indiana University, Bloomington, IN 47405.

E-mail address: arajca1@unl.edu

Table of Contents

1. Materials and Special Procedures.

Ether, tetrahydrofuran (THF), and 2-methyltetrahydrofuran (2-MeTHF) for use on the vacuum line were distilled from sodium/benzophenone prior to use. *t*-BuLi was obtained from either Aldrich (1.7 M in pentane) or Acros (1.5 M in pentane); prior to use, their concentrations were determined by titration with *N*-pivaloyl-*o*-toluidine.[S1] Other major commercially available chemicals were obtained from Aldrich. Column chromatography was carried out with flash silica gel, particle size 40–63 μm (EMD Chemicals). Deactivated silica was prepared by stirring flash silica gel with a solution of 2% Et_3N in pentane for 40 – 45 min. The silica gel was then transferred to a column and washed successively with pentane, acetone and pentane, following which it was dried overnight under a steady air pressure (~5 psi). This was then used for the column purifications in the usual way.

25,26,27,28–Tetrahydroxycalix[4]arene was obtained by $AlCl_3$–catalyzed removal of the *tert*-butyl groups from *p-tert*-butylcalix[4]arene according to the literature procedure.[S2] Preparation of 5,11,17,23-tetrabromo-25,26,27,28-tetrakis(methoxyethoxy)calix[4]arene (**4**) in the locked 1,3-alternate conformation is described below.

2. NMR Spectroscopy and Other Analyses.

NMR spectra were obtained using Bruker spectrometers (^{1}H, 500 MHz and 400 MHz) using $CDCl_3$ as solvent. The chemical shift references were as follows: (^{1}H) TMS, 0.0 ppm and (^{13}C) $CDCl_3$, 77.0 ppm. Typical 1D FID was subjected to exponential multiplication with an exponent of 0.1 Hz (for ^{1}H) and 1.0 – 2.0 Hz (for ^{13}C); for selected spectra, both exponential and Gaussian multiplications were used, with exponents indicated as EM and GB for each applicable spectrum.

Values of the magnetic moment and χT were obtained in chloroform using the ^{1}H NMR based Evans method.[S3] Concentric NMR tubes were used (Wilmad, cat. No. WGS-5BL). The outer NMR tube contained a solution of the paramagnetic sample in an approximately 1 : 1 (v/v) mixture of $CDCl_3$ and $CHCl_3$ with accurately determined concentration and the inner concentric tube contained pure $CHCl_3$.

Diamagnetic susceptibility of $CHCl_3$ ($\chi_{dia} = -0.497 \times 10^{-6}$ emu g^{-1}) and Pascal constant correction for the nitroxide diradical (-0.603×10^{-3} emu mol^{-1}) and tetraradical (-0.652×10^{-3} emu mol^{-1}) were used.[S4]

IR spectra were obtained using a Nicolet Avatar 360 FT-IR instrument, equipped with an ATR sampling accessory (Spectra Tech, Inc.). A few drops of the compound in CH_2Cl_2 were applied to the surface of a ZnSe ATR plate horizontal parallelogram (45°, Wilmad). After the solvent evaporated, the spectrum was acquired (128 scans, 4-cm^{-1} resolution).

MS analyses were carried out at the Nebraska Center for Mass Spectrometry.

Table S1. Summary of variable temperature ^{1}H NMR (400 MHz) spectroscopic studies of tetrahydroxylamine **5** (C_2Cl_4/benzene-d_6) and dihydroxylamine **6** (chloroform-*d*).

Chemical shifts (Hz)			Temperatures (° C)		k_{coal} (s^{-1})	$\Delta G^{\ddagger}$ (kcal mol^{-1})
ν_1	ν_2	$\nu_1-\nu_2$	$T_{slow\ exchange}$	$T_{coalescence}$		
Tetrahydroxylamine **5**						
2953.6	2685.2	268.4	25	52	597	14.8
Dihydroxylamine **6**						
2926.4	2907.2	19.2	−30	5	44.6	14.1
2953.2	2716.4	238.8	−30	33	526	14.1

3. X-ray Crystallography of 1 and 2.

All data were collected on Bruker SMART system at IUMSC (Indiana University). Data collection, structure solution, and refinement are briefly summarized below; more detailed description may be found in the accompanying crystallographic information files (CIFs). The single crystals for the X-ray crystallographic studies were obtained via slow evaporation of solvent at room temperature: nitroxide tetraradical **1** (label: SM-5-4recry) and diradical **2** (label: SM-5-5recry).

Data collection, structure solution and refinement. All data collections were carried out using Mo Kα radiation (λ = 0.71073 Å, graphite monochromator) at 137 K. The intensity data were corrected for absorption.[S5] Final cell constants were calculated from the xyz centroids of strong reflections from the actual data collection after integration.[S6]

Space groups were determined based on intensity statistics and systematic absences. Structures were solved with direct methods using SIR-92[S7] and refined with full-matrix least squares / difference Fourier cycles using SHELXL-97.[S8] All non-hydrogen atoms were refined with anisotropic displacement parameters. The hydrogen atoms were placed in ideal positions and refined as riding atoms with relative isotropic displacement parameters.

Nitroxide tetraradical 1. The compound crystallized in space group P21/c with one molecule per asymmetric unit. The final full matrix least squares refinement converged to R1 = 0.0461 and wR2 = 0.1276 (F2, all data). The remaining electron density was located on bonds.

Nitroxide diradical 2. The compound crystallized in space group P-1 with two molecules and one half solvent molecule (benzene) per asymmetric unit. The final full matrix least squares refinement converged to R1 = 0.0483 and wR2 = 0.1257 (F2, all data). The remaining electron density is located near the bromine atoms. Disorder was observed for a *tert*-butyl group and methoxyethylene; they were refined with a set of appropriate restraints and constraints.

Table S2. Dihedral angles between the planes defined by the C(*ipso*)-C(CH_2)-C(*ipso*) and benzene ring planes (illustrated as triangles and hexagons) for nitroxide tetraradical **1** and diradical **2**.

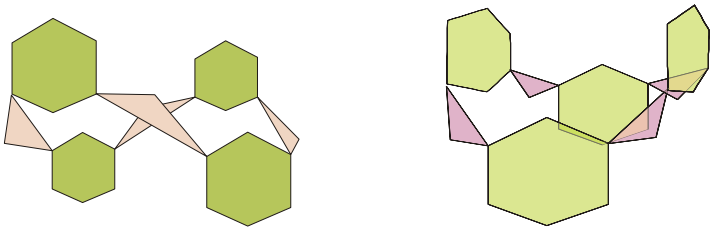

Nitroxide tetraradical **1**

Plane to plane (defined by the following carbon atoms)	Angle (plane to plane) [°]
Ph 1-6 to 5,7,8	115.7 (or 64.3)
5,7,8 to Ph 8-13	118.4 (or 61.6)
Ph 8-13 to 12,14,15	114.3 (or 65.7)
12,14,15 to Ph 15-20	61.5
Ph 15-20 to 19,21,22	67.5
19,21,22 to Ph 22-27	64.3
Ph 22-27 to 26,28,1	67.9
26,28,1 to Ph 1-6	120.8 (or 59.2)

Nitroxide diradical **2**

Molecule A

Plane to plane (defined by the following carbon atoms)	Angle (plane to plane) [°]
Ph 1-6 to 5,7,8	68.0
5,7,8 to Ph 8-13	70.2
Ph 8-13 to 12,14,15	107.4 (or 72.6)
12,14,15 to Ph 15-20	65.0
Ph 15-20 to 19,21,22	65.1
19,21,22 to Ph 22-27	69.9
Ph 22-27 to 26,28,1	72.4
26,28,1 to Ph 1-6	114.4 (or 65.6)

Molecule B

Plane to plane (defined by the following carbon atoms)	Angle (plane to plane) [°]
Ph 1-6 to 5,7,8	111.6 (or 68.4)
5,7,8 to Ph 8-13	70.3
Ph 8-13 to 12,14,15	73.4
12,14,15 to Ph15-20	66.1
Ph 15-20 to 19,21,22	113.9 or 66.1
19,21,22 to Ph 22-27	69.4
Ph 22-27 to 26,28,1	70.0
26,28,1 to Ph 1-6	70.4

4. EPR Spectroscopy of 1 and 2, and Magnetic Studies of 1, 2, and 3.

EPR spectroscopy. CW X-band EPR spectra for **1** and **2** in solution were acquired on Bruker EMX instrument, equipped with a frequency counter and nitrogen flow temperature control (130–320 K). The samples were contained in the 4-mm O.D. EPR quartz tubes, equipped with high-vac PTFE stopcocks. Solvent was vacuum transferred into the tube, to form a homogeneous solution after attaining ambient temperature. Spectra were obtained using dual mode cavity, with the oscillating magnetic field perpendicular (TE_{102}) to the swept magnetic field. The *g*-values were referenced using DPPH (g = 2.0037, powder, Aldrich).

For distance (r, in Å) measurements based upon Eaton's equation (eq. S1), the relative intensities of the the $|\Delta m_s| = 1$ and $|\Delta m_s| = 2$ regions for 1 mM diradical **2** in toluene/chloroform were obtained by double integration with baseline correction; intensity of the monoradical was negligible. The instrument settings for the $|\Delta m_s| = 2$ region were as follows: microwave (MW) power attenuation = 10 dB (power = 20.4 mW) and receiver gain = 5×10^5; analogous settings for the $|\Delta m_s| = 1$ region were 40 dB (2.046×10^{-2} mW) and 1×10^5. Except for the center fields, all other settings, including MW frequency (ν = 9.4848 GHz), modulation amplitude (2 G), number of scans, and sweep width (600 G), were identical.

$$\text{relative intensity} = [19.5 \times (9.1)^2]/r^6\nu^2 \qquad \text{(S1)}$$

SQUID Magnetometry. Quantum Design (San Diego, CA) MPMS5S (with continuous temperature control) was used. All samples were contained in home-made 5-mm O.D. EPR quality quartz tubes, modified to possess a thin bottom, which is 6 cm from the end of the tube.[S9]

For solution samples, tetraradical **1**, diradical **2**, or tetraradical **3** were loaded into the tube, placed under vacuum, and then solvents were vacuum transferred. The tube was flame sealed under vacuum. The samples were carefully inserted to the magnetometer, with the sample chamber at 290–300 K. The sequence of measurements started with a cooling mode from 300 K to 1.8 K, and then followed with the other sequences of measurements below the melting point of the solution (1.8–150 K). Correction for diamagnetism was carried out by extrapolation of the χ vs. $1/T$ plots, typically, from the 60–140 K

temperature range (R^2 = 0.9999). However, for selected samples in 2-methyltetrahydrofuran, a wider temperature range (up to the temperature of 240 K) was used. Usually the cooling mode data, with 10–60 s delays, after a "stable temperature" was indicated by the MPMS at each temperature, were used for such extrapolations.

For solid state samples, **1** or **2** was loaded to the tube, placed under vacuum, and then flame sealed under partial pressure of helium gas. For one of the samples of tetraradical **1** (Figure 12), following the measurements, the SQUID sample tube was opened and cleaned, and then identical sequences of measurements were carried out for the point-by-point correction for diamagnetism; additional corrections were based upon Pascal constants, scaled by a factor of 0.9, i.e., $\chi_{dia} = 0.9\times6.52\times10^{-4}$ emu mol^{-1}. For all other samples of solid di- and tetraradicals, the correction for diamagnetism was based upon high temperature extrapolation of the χ vs. $1/T$ plots, i.e., a suitable numerical factor (M_{dia}) was added to the magnetization (M), until the χT vs. T plot becomes flat in the high temperature range.

EPR Spectral Simulations and Numerical Curve Fitting for SQUID Magnetic Data. The WINEPR SimFonia program (Version 1.25, Bruker) was used for spectral simulations of nitroxide diradical **2** in rigid matrices. WinSIM program (Public EPR Software Tools, D. A. O'Brien, D. R. Duling, Y. C. Fann) was used for numerical fitting of solution phase EPR spectra.

The SigmaPlot for Windows software package was used for numerical curve fitting of the magnetic data. The reliability of a fit is measured by the parameter dependence, which is defined as follows: *dependence = 1 – ((variance of the parameter, other parameters constant)/(variance of the parameter, other parameters changing))*. Values close to 1 indicate an overparametrized fit. The quality of fits is measured by a coefficient of determination (R^2), which is defined for nonlinear numerical fits of the magnetic data as follows (eq. S2):

$$R^2 = 1 - [(\Sigma(y_i - Y_i)^2)/(\Sigma(y_i - \langle y \rangle)^2)] \qquad \text{(S2)}$$

where y_i, Y_i , and $\langle y \rangle$ denote experimental values, fitted values, and the arithmetic mean of the experimental values. Values close to 1 indicate a fit of high quality.

5. Alternative Models for Numerical Fitting of Magnetic Data for Tetraradical 1 and Diradical 2.

Two diradicals model. In this model, it is assumed that all nitroxide moieties are involved in only one dominant pairwise antiferromagnetic exchange coupling (J/k). For isolated **1** and **2**, this model describes pairwise exchange couplings between the diagonal nitroxides only. For solid **1** and **2**, the four nitroxide moieties are described as two diradicals. For tetraradical **1**, equations for the field-dependence of magnetization (M vs. H) and temperature dependence of magnetic susceptibility (χT vs. T) are provided (eq. S3, eq. S4a). N denotes the number of moles of tetraradical **1** (eq. S3). Also, impurities and inaccuracies in the mass balance are accounted for by the "magnetization at saturation," M_{sat} (eq. S3) and the mass factor, w (eq. S4a). Both equations account for paramagnetic saturation. A similar model may be used to fit the χT vs. T data for diradical **2** (eq. S4b).

$$M = (11180N)M_{sat}[F_1 + F_2] \quad \text{(S3)}$$

$$\chi T = (1.118T/H)w[F_1 + F_2] \quad \text{(S4a)}$$

$$\chi T = (1.118T/2H)w[F_1 + F_2] \quad \text{(S4b)}$$

$$F_n = [2\sinh(a)]/[1 + 2\cosh(a) + \exp((-2J_n/k)/T)];\ n = 1, 2$$

$$a = 1.345(H/T);\ J_1 = J_2$$

It should be noted that the replacement of the $J_2 = 0$ restraint in equations S5, S6a, and S6b with a $J_1 = J_2$ restraint gives equations S3, S4a, and S4b. Also, setting $J_1 = 0$ in the tetraradical model (eq. 1, 2, and 4, maint text) gives equations (and numerical fits) that are identical to equations S3, S4a, and S4b. Still another option is a three-parameter fit, using eq. S4a with $J_1 \neq J_2$ (e.g., ref 32, main text), for tetraradical **1**.

Diradical plus two S = ½ monoradicals model. In this model, it is assumed that one half of the nitroxide moieties may be described as exchange-coupled diradicals and the other half of the nitroxide moieties are treated as independent S = ½ monoradicals. In other words, the four nitroxide moieties in solid **1** and **2** could be described as one diradical plus two S = ½ monoradicals.

For tetraradical **1**, both temperature-dependence (χT vs. T) and field-dependence (M vs. H) of the experimental magnetic data are well fit by the model of "one diradical plus two S = ½ monoradicals", with antiferromagnetic exchange coupling (J/k) in the "diradical" (eq. S5 and eq. S6a). N denotes number of moles of tetraradical **1** (eq. S5). Also, impurities and inaccuracies in the mass balance are accounted for by the "magnetization at saturation," M_{sat} (eq. S5) and the mass factor, w (eq. S6a). Both equations account for paramagnetic saturation. Similar model may be used to fit the χT vs. T data for diradical **2** (eq. S6b).

$$M = (11180N)M_{sat}[F_1 + F_2] \quad \text{(S5)}$$

$$\chi T = (1.118T/H)w[F_1 + F_2] \quad \text{(S6a)}$$

$$\chi T = (1.118T/2H)w[F_1 + F_2] \quad \text{(S6b)}$$

$$F_n = [2\sinh(a)]/[1 + 2\cosh(a) + \exp((-2J_n/k)/T)];\ n = 1, 2$$

$$a = 1.345(H/T);\ J_2 = 0$$

Two-parameter numerical fits (eq. S5, S6a, and S6b) for tetraradical **1** and diradical **2** give similar antiferromagnetic exchange coupling, $J/k \approx -1.8$ K, between isolated pairs of nitroxide moieties.

6. Preparation of Tetrabromocalix[4]arene 4.

25,26,27,28-Tetrakis(methoxyethoxy)calix[4]arene. To a mixture of 2-methoxyethanol (22.85 g, 300 mM, sm-4-19) and 40 mL of dry pyridine, *p*-TsCl (63 g, 330 mM) was added in portions, in such a way that the temperature of the reaction mixture did not exceed 20 ºC. The stirring was continued for 6 h, after which the reaction mixture was taken up in ether and water, and then the ether layer was washed thoroughly with water. Then it was dried over $MgSO_4$ and the ether was removed under reduced pressure. The resulting 2-methoxyethyl tosylate (yellow oil) was used without further purification. Similarly, four additional reactions (sm-4-27, sm-4-89, sm-6-53, sm-6-72) on 25-g scales gave the crude

product with the estimated purity of 90–92% by ^{1}H NMR spectroscopy. The yields of these crude products were in the 60–72% range.

A mixture of 25,26,27,28-tetrahydroxycalix[4]arene (2.00 g, 4.71 mmol) and Cs_2CO_3 (46.1 g, 0.141 mol) in DMF (110 mL) was stirred at 80 °C for 30 min. Subsequently 2-methoxyethyl tosylate (32.7 g, 0.141 mol) was added and the reaction mixture was kept at 80 °C for 5 h. Upon cooling to ambient temperature, the reaction mixture was poured into water (400 mL). After extraction with CH_2Cl_2 (3 × 125 mL), the combined organic layers were washed with 1 N HCl (1 × 125 mL) and brine (3 × 125 mL). In order to remove the excess tosylate, a mixture of the resulting residue, KI (2 g), and Et_3N (2 mL) in CH_3CN (60 mL) was refluxed for 1 h. The solvent was removed in vacuo. CH_2Cl_2 (100 mL) was added to the residue whereupon the organic layer was washed with 1 N HCl (1 × 100 mL) and water (2 × 125 mL). The organic layer was dried over $MgSO_4$. Concentration in vacuo gave a brown gel-like solid which was triturated with cold MeOH to afford a white solid (1.39 g, 45%, m.p. 197–199 °C; lit.[S10] 198–200 °C). In three additional reactions carried out on 1-g, 1.5-g, and 0.1-g scale, the product of trituration was further recrystallized from CH_2Cl_2/MeOH, to provide the product in 46–48% (lit.[S10] 76%) yields. ^{1}H NMR (500 MHz, $CDCl_3$): 7.070 (d, J = 7.0, 8H), 6.710 (t, J = 7.0, 4H), 3.786 (t, J = 5.0, 8H), 3.478 (t, J = 5.0, 8H), 3.648 (s, 8H), 3.388 (s, 12H).

5,11,17,23-Tetrabromo-25,26,27,28-tetrakis(methoxyethoxy)calix[4]arene (4).[S11] N-bromosuccinimide (5.7 g, 31.9 mmol) and 25,26,27,28-tetrakis(methoxyethoxy)calix[4]arene (2.38 g, 3.62 mmol) in methyl ethyl ketone (115 mL) were stirred at room temperature for 24 h. Subsequently, $NaHSO_3$ (5 mL, 10% in water) was added to the stirred reaction mixture. The aqueous workup with CH_2Cl_2 (25 mL), drying over $MgSO_4$, concentration in vacuo, and recrystallization of the crude in CH_2Cl_2/MeOH gave white crystals (2.92 g, 83%, m.p. 255 °C, sm-6-60). From other five reactions carried out on 100-mg (sm-4-34), 588-mg (sm-4-40), 750-mg (sm-4-88), 1.4-g (sm-5-7), and 1.3-g (sm-5-97) scale, tetrabromocalix[4]arene **4** was obtained in 81–93% yields. The higher yields correspond to the crude mixtures, which were of sufficient purity (>95% based upon ^{1}H NMR spectra) for the

subsequent steps in the synthesis. ^{1}H NMR (500 MHz, $CDCl_3$, sm-6-60recry1): 7.312 (s, 8H), 3.853 (m, 8H), 3.734 (m, 8H), 3.595 (s, 8H), 3.456 (s, 12H). ^{13}C NMR (125 MHz, $CDCl_3$, sm-6-60recry1): 154.6, 134.6, 133.2, 114.9, 71.94, 71.91, 59.3, 34.1. IR (ZnSe, cm^{-1}, sm-6-60recry1): 2918, 2880, 1577, 1450, 1365, 1195, 1130, 1050, 852. LR/HR FABMS (3-NBA, sm-6-60recry1): m/z (ion type, % RA in the *m*/*z* 700–1400, deviation for the formula) at 975.9721 ($[M+8]^+$, 29, –3.5 ppm for $^{12}C_{40}H_{44}{}^{16}O_8{}^{81}Br_4$), 973.9657 ($[M+6]^+$, 61, 5.2 ppm for $^{12}C_{40}H_{44}{}^{16}O_8{}^{81}Br_3{}^{79}Br$), 971.9660 ($[M+4]^+$, 100, 7.0 ppm for $^{12}C_{40}H_{44}{}^{16}O_8{}^{81}Br_2{}^{79}Br_2$), 969.9664 ($[M+2]^+$, 62, 8.8 ppm for $^{12}C_{40}H_{44}{}^{16}O_8{}^{81}Br^{79}Br_3$), 967.9737 ($[M]^+$, 16, 3.3 ppm for $^{12}C_{40}H_{44}{}^{16}O_8{}^{79}Br_4$).

7. Acknowledgment

The packing plots in Figures S1 – S3 were prepared using Mercury1.3 program from CCDC.

8. References for Supporting Information

S1. Suffert, J. *J. Org. Chem.* **1989**, *54*, 509–510.

S2. Gutsche, C.D.; Levine, J. A., Sujeeth, P. K. *J. Org. Chem.* **1985**, *50*, 5802–5806.

S3. Evans, D. F. *J. Chem. Soc.* **1959**, 2003–2005. Live, D. H.; Chan, S. I. *Anal. Chem.* **1970**, *42*, 791–792.

S4. *Handbook of chemistry and physics*, CRC Press, INC, Florida, 1983–1984, 64th Ed., E-114.

S5. SADABS: Blessing, R. *Acta Cryst. A* **1995**, *51*, 33–38).

S6. SAINT 6.1, Bruker Analytical X-Ray Systems, Madison, WI, **1999**.

S7. SIR-92: Altomare, A.; Cascarno, G.; Giacovazzo, C.; Gualardi, A. *J. Appl. Cryst.* **1993**, *26*, 343–350.

S8. SHELXL-97: SHELXTL-Plus V5.10, Bruker Analytical X-Ray Systems, Madison, WI

S9. Rajca, A.; Pink, M.; Rojsajjakul, T.; Lu, K.; Wang, H.; Rajca, S. *J. Am. Chem. Soc.* **2003**, *125*, 8534–8538.

S10. Verboom, W.; Datta, S.; Reinhoudt, D. N. *J. Org. Chem.* **1992**, *57*, 5394–5398.

S11. Mislin, G.; Graf, E, Hosseini, M. W.; Cian, A. D.; Kyritsakas, N. *Chem. Commun.* **1998**, 2545–2546.

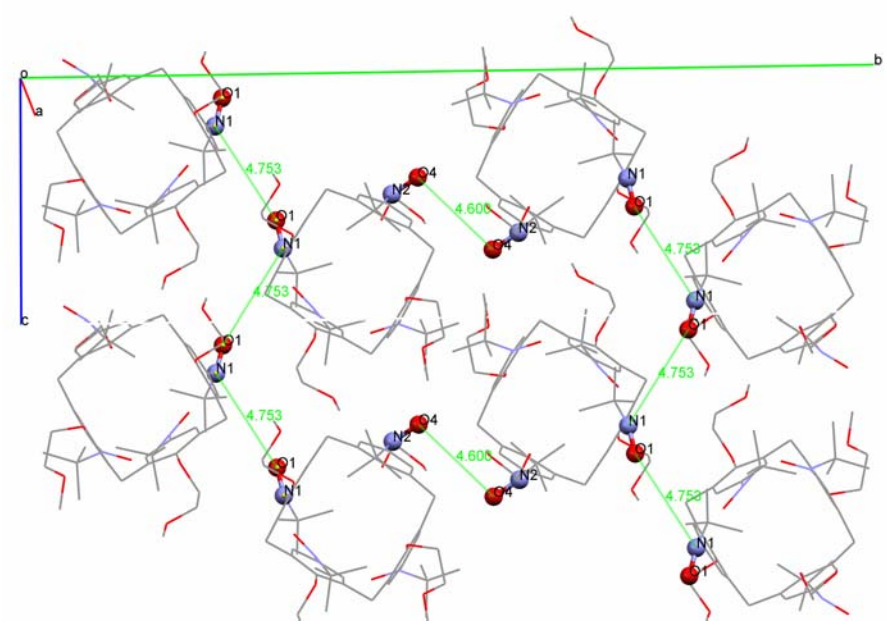

Figure S1. Crystal packing of **1** as viewed in the approximate direction of the crystallographic *a*-axis. The NO groups, with the short intermolecular O···O and N···O distances of 4.60 and 4.75 Å, are shown in ball-and-stick. Hydrogen atoms are omitted for clarity.

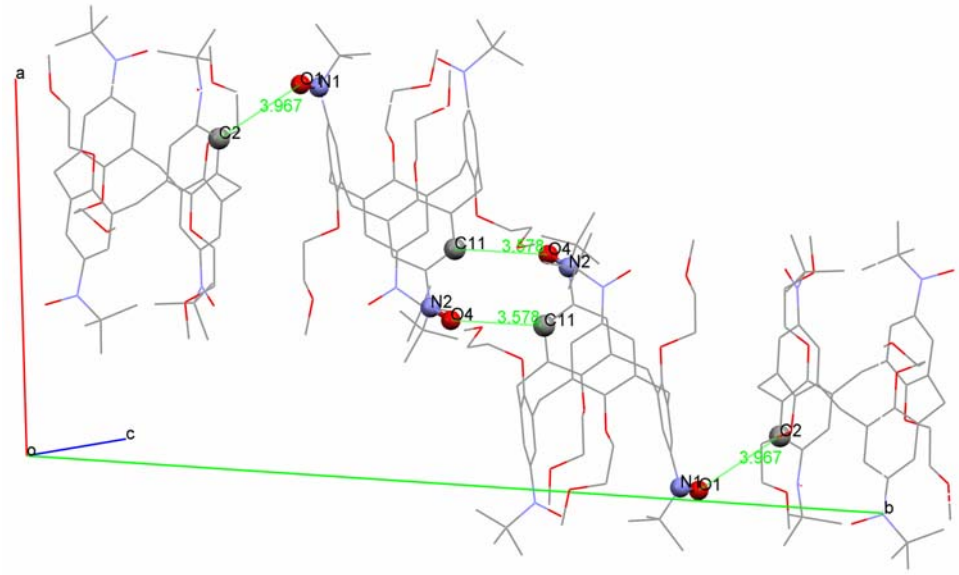

Figure S2. Crystal packing of **1** as viewed in the approximate direction of the crystallographic *c*-axis. The NO groups and carbon atoms, with the short intermolecular O···C distances (O1···C2 = 3.97 Å and O4···C11 = 3.58 Å), are shown in ball-and-stick. Hydrogen atoms are omitted for clarity.

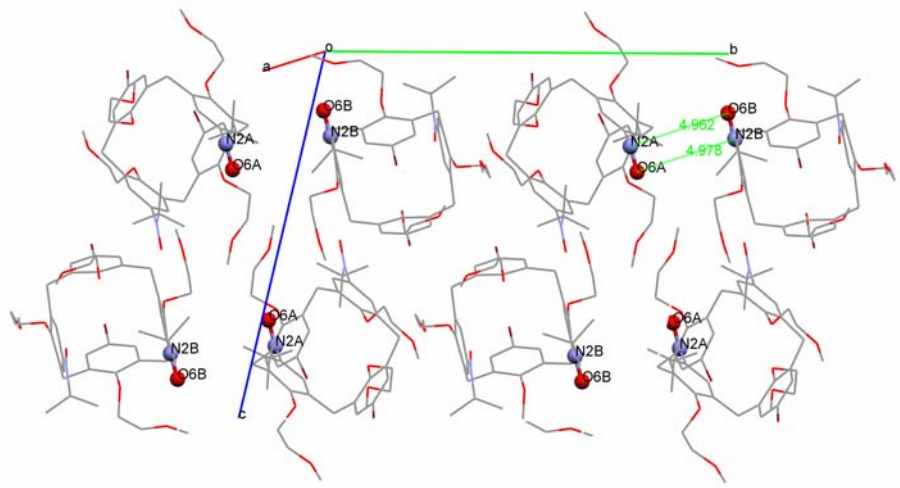

Figure S3. Crystal packing of **2** as viewed in the approximate direction of the crystallographic *a*-axis. The NO groups forming intermolecular dimers are shown in ball-and-stick; the short intermolecular N···O distances of 4.96 and 4.98 Å are found. Both angles and torsions are within 5° of the values expected for a rectangular arrangement of the NO groups within the dimer. Hydrogen atoms, disorder, and solvent of crystallization (benzene) are omitted for clarity.

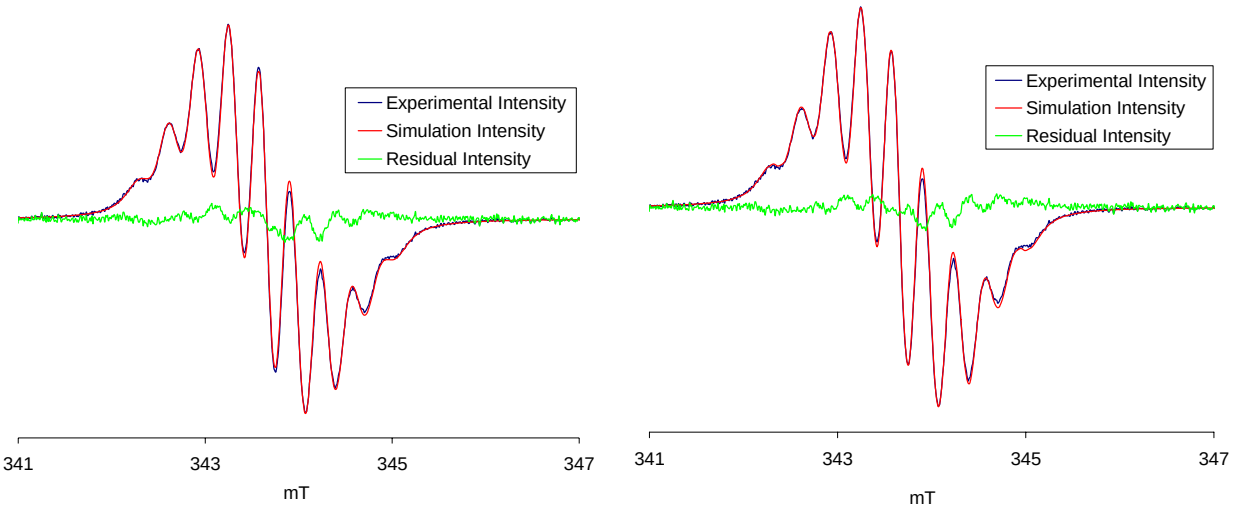

Figure S4. EPR (X-band) spectra of 1 mM nitroxide tetraradical **1** in toluene at room temperature.

Left spectrum, red trace: single species numerical fit (R = 0.999, WinSim), as shown in Figure 6 (main text), with the following variable parameters [rel. concentration, Lorentzian percentage, line width, g-shift (g-value), ^{14}N-splitting (spin, number), ^{1}H-splitting (spin, number)]: species no. 1 [100, 100%, 1.560, −0.450 (2.0059), 3.190 (1, 4), 0.480 (0.5, 8)]. Right spectrum (ks980r2), red trace: three-species numerical fit (R = 0.999, WinSim) with the following variable parameters [rel concentration, Lorentzian percentage, line width, g-shift (g-value), ^{14}N-splitting (spin, number), ^{1}H-splitting (spin, number)]: species no. 1 [98.7, 100%, 1.510, −0.450 (2.0059), 3.190 (1, 4), 0.490 (0.5, 8)], species no. 2 [1.1, 100%, 1.510, −0.400 (2.0058), 4.330 (1, 3), 0.620 (0.5, 6)], species no. 3 [0.2, 100%, 0.510, −0.500 (2.0059), 6.570 (1, 2), 0.800 (0.5, 4)]. The line widths, g-shifts, and hyperfine splittings are reported in Gauss. Green trace: Residual Intensity (the difference between Experimental Intensity and Simulation Intensity multiplied by a factor of 2).

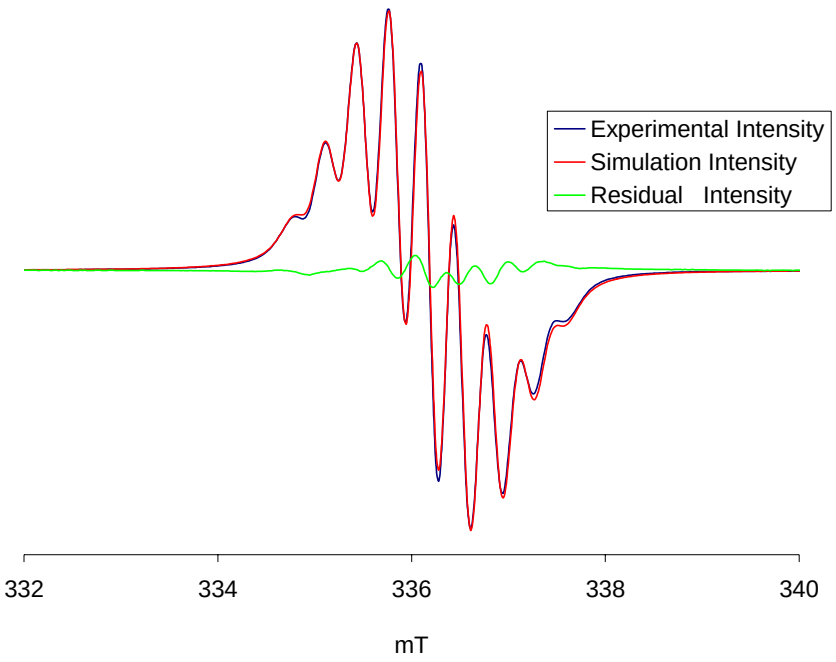

Figure S5. EPR (X-band) spectra of 0.6 mM nitroxide tetraradical **1** in toluene/chloroform (4 : 1) at 296 K (PT366r1). Red trace: single species numerical fit (R = 0.999, WinSim), with the following variable parameters [rel. concentration, Lorentzian percentage, line width, g-shift (g-value), ^{14}N-splitting (spin, number), ^{1}H-splitting (spin, number)]: species no. 1 [100, 100%, 1.680, 3.780 (2.0056), 3.290 (1, 4), 0.390 (0.5, 8)]. The line widths, g-shifts, and hyperfine splittings are reported in Gauss. Green trace: Residual Intensity (Experimental Intensity−Simulation Intensity)

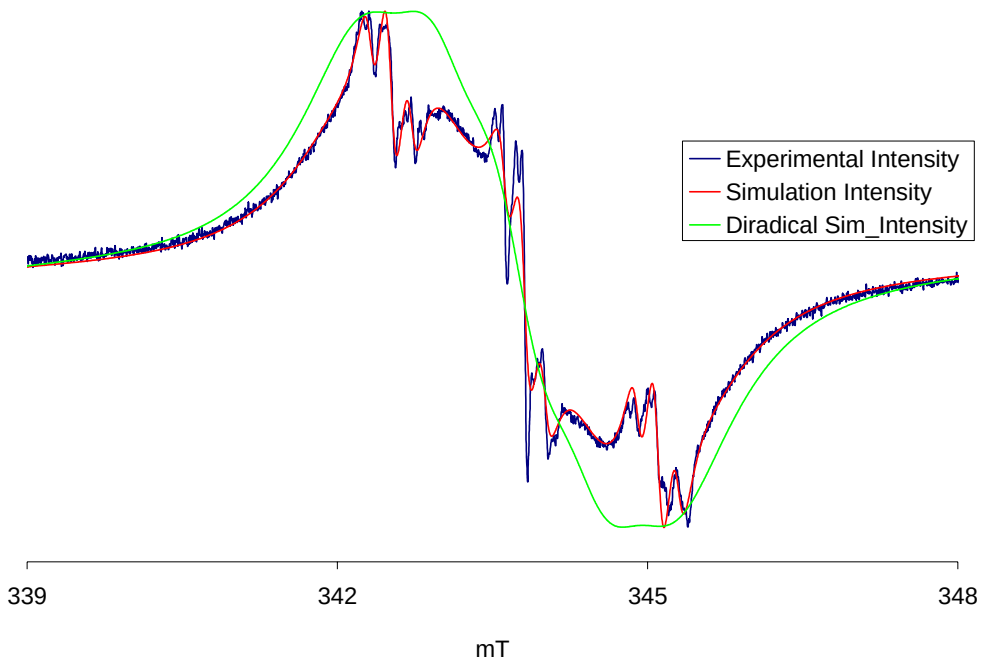

Figure S6. EPR (X-band) spectrum of 1.1 mM nitroxide diradical **2** in toluene at 295 K (KS1263r3). Red trace: numerical fit (R = 0.994, WinSim) with the following variable parameters [rel concentration, Lorentzian percentage, line width, g-shift (g-value), ^{14}N-splitting (spin, number), ^{1}H-splitting (spin, number)]: species no. 1 [97.880, 100%, 7.860, −0.550 (2.0064), 6.520 (1, 2)], species no. 2 [2.120, 80%, 1.080, 0.070 (2.0060), 12.910 (1, 1), 1.970 (0.5, 2)]. The ^{1}H-splitting for the diradical was not included. The line widths, g-shifts, and hyperfine splittings are reported in Gauss. Green trace: numerical fit for species no. 1 in isolation with above optimized parameters.

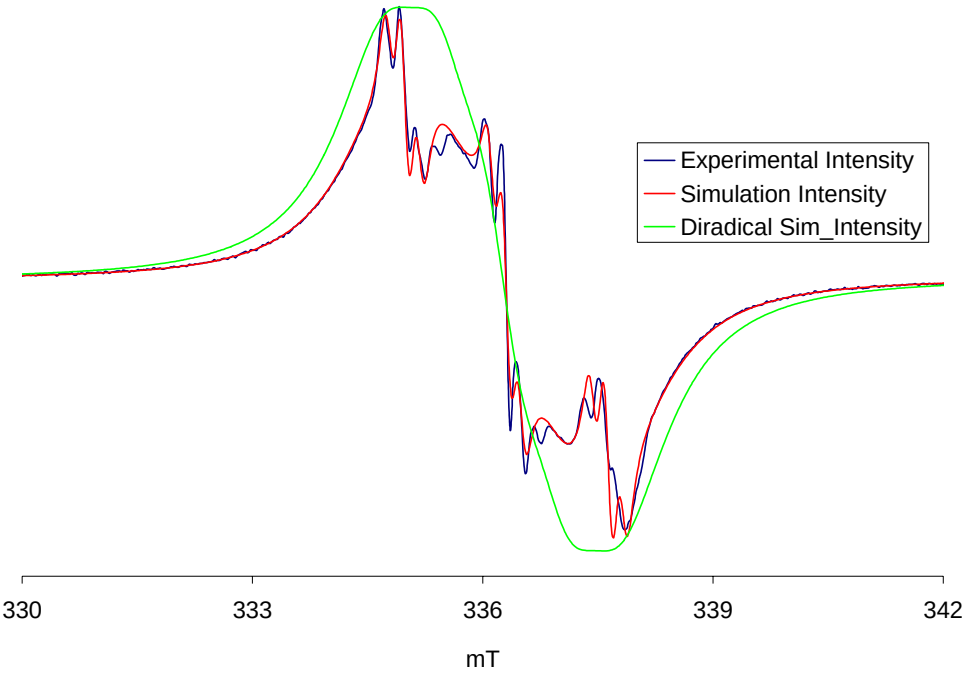

Figure S7. EPR (X-band) spectrum of 0.65 mM nitroxide diradical **2** in toluene/chloroform (4 : 1) at 296 K (PT364r1). Red trace: numerical fit (R = 0.995, Winsim) with the following variable parameters [rel concentration, Lorentzian percentage, line width, g-shift (g-value), ^{14}N-splitting (spin, number), ^{1}H-splitting (spin, number)]: species no. 1 [97.060, 99%, 8.290, 4.520 (2.0061), 6.570 (1, 2)], species no. 2 [2.940, 93%, 1.110, 5.000 (2.0058), 13.230 (1, 1), 1.890 (0.5, 2)]. The ^{1}H-splitting for the diradical was not included. The line widths, g-shifts, and hyperfine splittings are reported in Gauss. Green trace: numerical fit for species no. 1 in isolation with above optimized parameters. (Using DPPH standard, g = 2.0058 is obtained.)

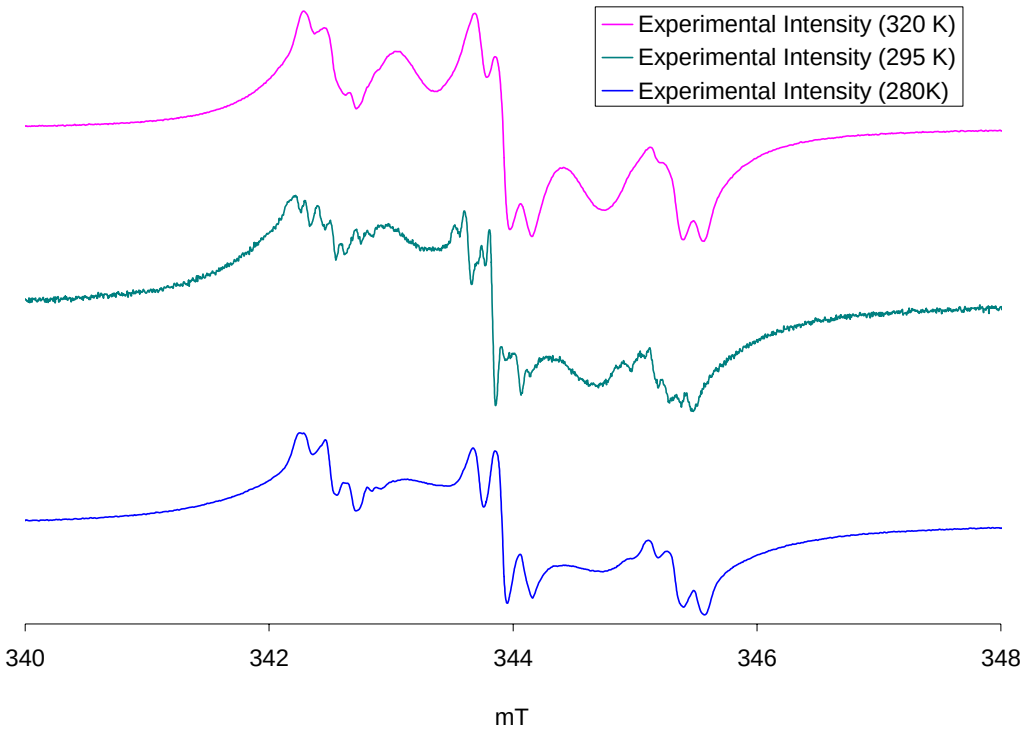

Figure S8. EPR (X-band) spectra of 1 mM nitroxide diradical **2** in DCM/MeOH (4 : 1). Purple trace (topmost): spectrum at 320 K (KS765r6). Green trace (center): spectrum at 295 K (KS1263r5). Blue trace (lowermost): spectrum at 280 K (KS765r4). Identical sample was used for spectra at 280 K and 320 K.

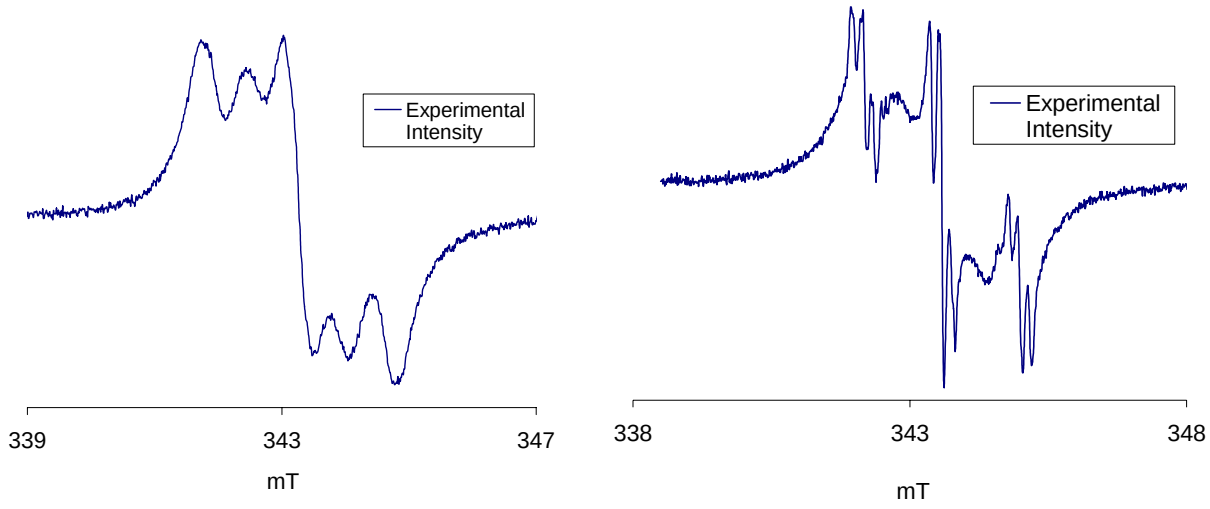

Figure S9. EPR (X-band) spectra of 1 mM nitroxide diradical **2** at room temperature. Left spectrum: **2** in acetonitrile (KS955r2). Right spectrum: **2** in dichloromethane at 297 K (KS970r2).

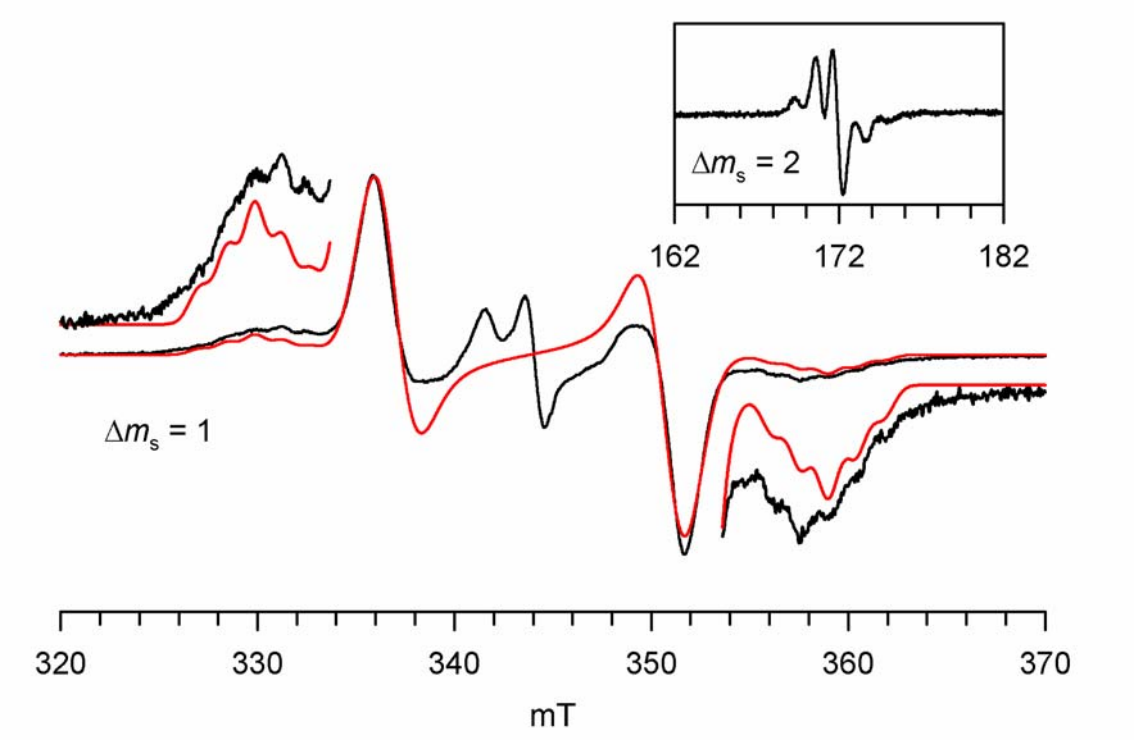

Figure S10. EPR (X-Band, 9.6561 GHz) spectrum of 1 mM nitroxide diradical **2** in dichloromethane/methanol (4 : 1) at 140 K (label: KS1263r14). The spectral simulation of the $|\Delta m_s| = 1$ region is shown as red trace. The fitting parameters for the spectral simulation for the $S = 1$ state are: $|D/hc| = 1.36 \times 10^{-2}$ cm^{-1} ($D = 145$ G), $|E/hc| = 0$ cm^{-1}, $g_x = 2.0062$, $g_y = 2.0062$, $g_z = 2.0035$, $|A_{zz}/2|/hc \approx 1.3 \times 10^{-3}$ cm^{-1}, Gaussian line ($L_x = 20$ G, $L_y = 22$ G, $L_z = 12$ G). The center lines correspond to an $S = ½$ (monoradical) impurity.

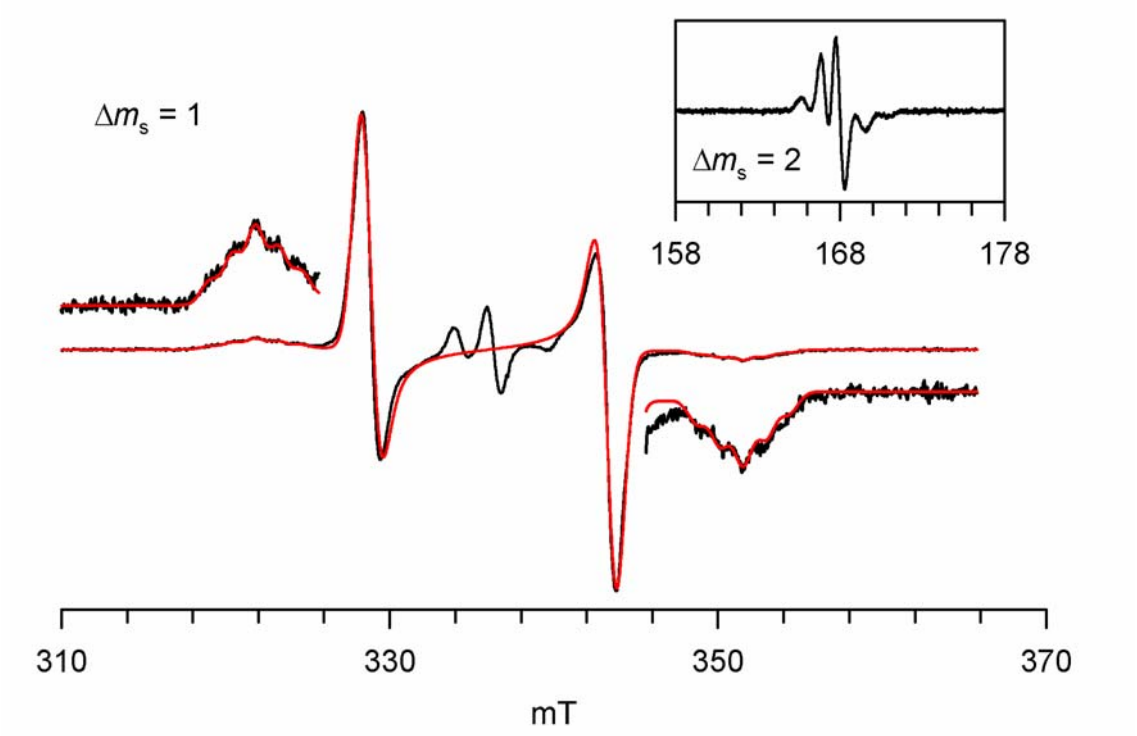

Figure S11A. EPR (X-Band, 9.4389 GHz) spectrum of 0.7 mM nitroxide diradical **2** in 2-MeTHF at 140 K (label: PT363r2/r4). The spectral simulation of the $|\Delta m_s| = 1$ region is shown as red trace. The fitting parameters for the spectral simulation for the $S = 1$ state are: $|D/hc| = 1.39 \times 10^{-2}$ cm^{-1} ($D = 149$ G), $|E/hc| = 0$ cm^{-1}, $g_x = 2.0064$, $g_y = 2.0064$, $g_z = 2.0031$, $|A_{zz}/2|/hc \approx 1.3 \times 10^{-3}$ cm^{-1}, and Gaussian line ($L_x = 11$ G, $L_y = 13$ G, $L_z = 11$ G). The center lines correspond to an $S = ½$ (monoradical) impurity.

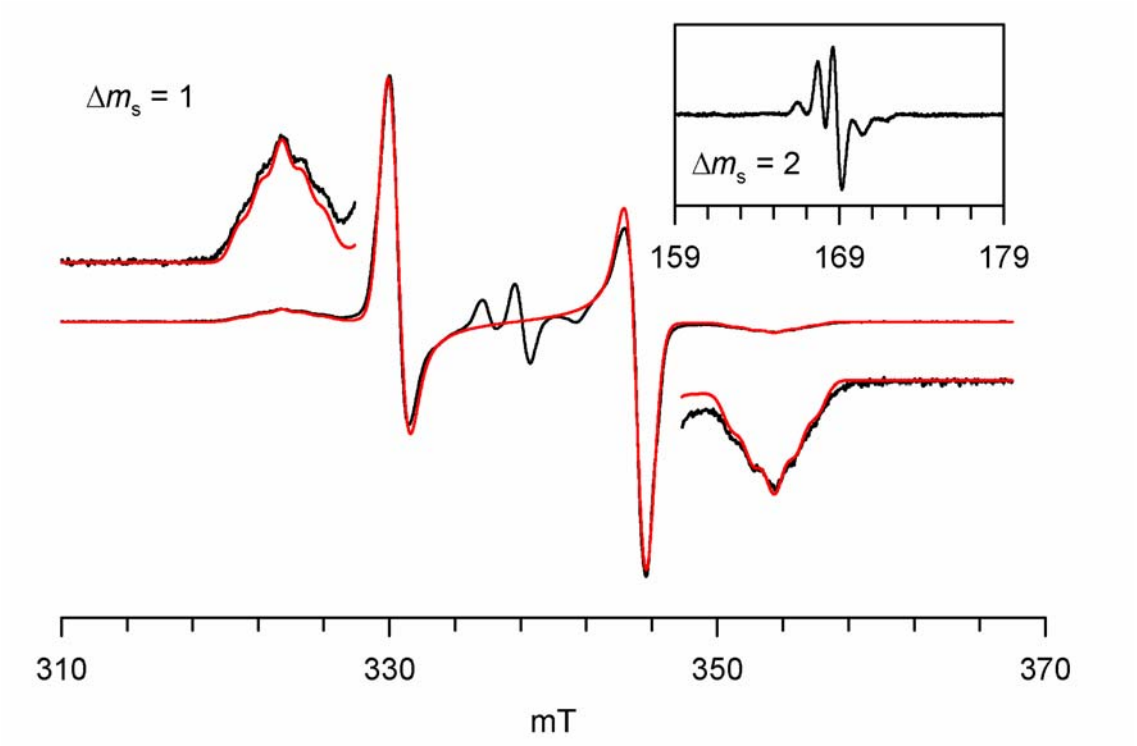

Figure S11B. EPR (X-Band, 9.4876 GHz) spectrum of 0.7 mM nitroxide diradical **2** in 2-MeTHF at 135 K (label: SM1112r4/r5). The spectral simulation of the $|\Delta m_s| = 1$ region is shown as red trace. The fitting parameters for the spectral simulation for the $S = 1$ state are: $|D/hc| = 1.405 \times 10^{-2}$ cm^{-1}, $|E/hc| = 0$ cm^{-1}, $g_x = 2.0063$, $g_y = 2.0063$, $g_z = 2.0028$, $|A_{zz}/2|/hc \approx 1.2 \times 10^{-3}$ cm^{-1}, and Gaussian line ($L_x = 11$ G, $L_y = 13$ G, $L_z = 11$ G). The center lines correspond to an $S = ½$ (monoradical) impurity.

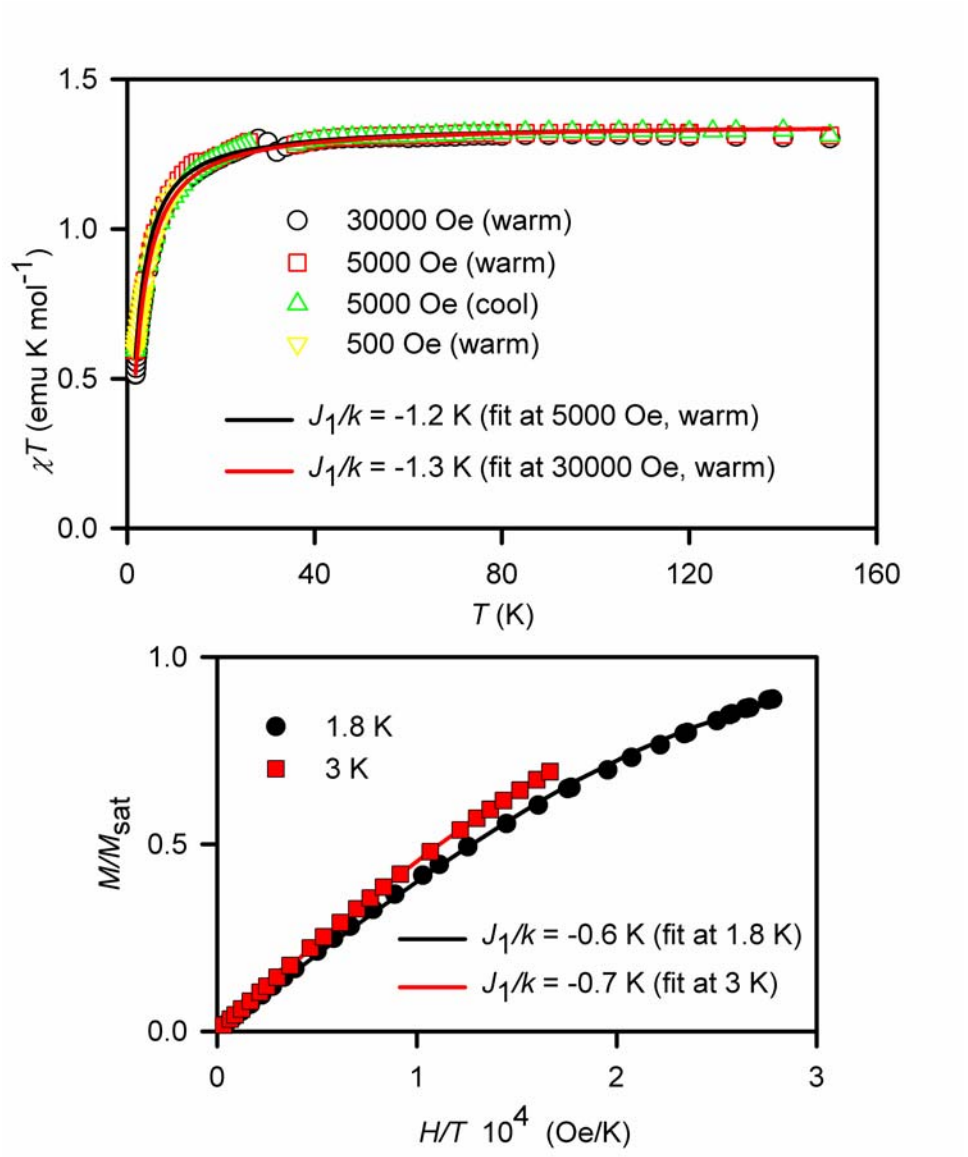

Figure S12. SQUID magnetometry for concentrated (13 mM) solution of **1** in THF (label: SM988r1F) with numerical fits to the tetraradical model (Figure 10, eq. 1 and 2). For the χT vs. T fits (top) and the M/M_{sat} vs. H/T fits (bottom), the J_2/k (diagonal coupling) is set to –1.1 K and –0.6 K, respectively. The variable parameters (parameter dependence and R^2) are as follows: at 30000 Oe in the warming mode, J_1/k = –1.3 K, w = 0.90 (0.32, 0.998); at 5000 Oe in the warming mode, J_1/k = –1.2 K, w = 0.90 (0.30, 0.995); at 1.8 K, J_1/k = –0.6 K, M_{sat} = 0.62 μ_B (0.86, 0.999); at 3 K, J_1/k = –0.7 K, M_{sat} = 0.70 μ_B (0.97, 1.000).

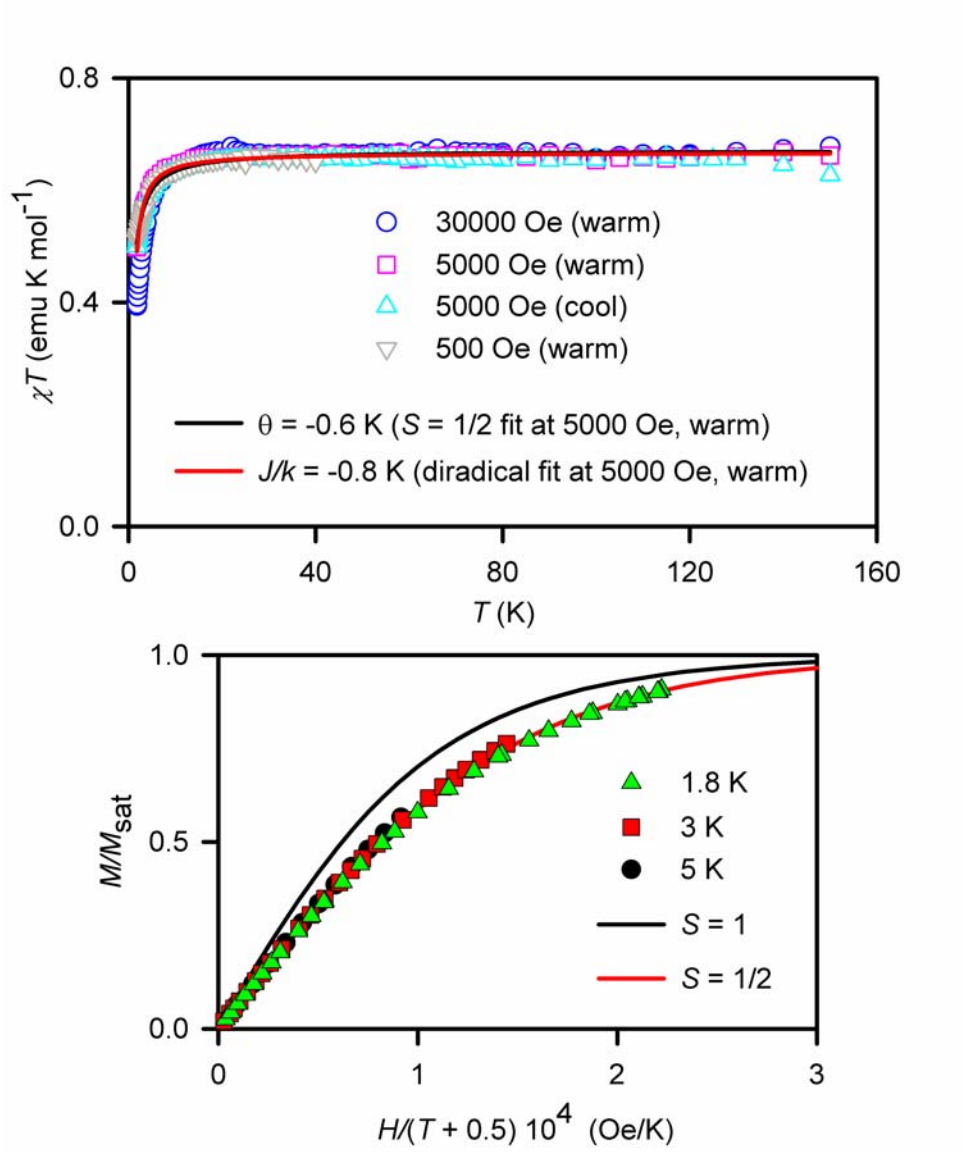

Figure S13. SQUID magnetometry for dilute (7 mM) solution of nitroxide diradical **2** in THF (label: KD1256F). The experimental data are identical to that in Figure 9 (main text). The mean-field numerical fits (θ = –0.5 K or θ = –0.6 K) are shown. For the χT vs. T data, numerical fit to the diradical model is shown for reference. In the magnetization plot, the solid lines correspond to Brillouin functions with $S = ½$ and $S = 1$.

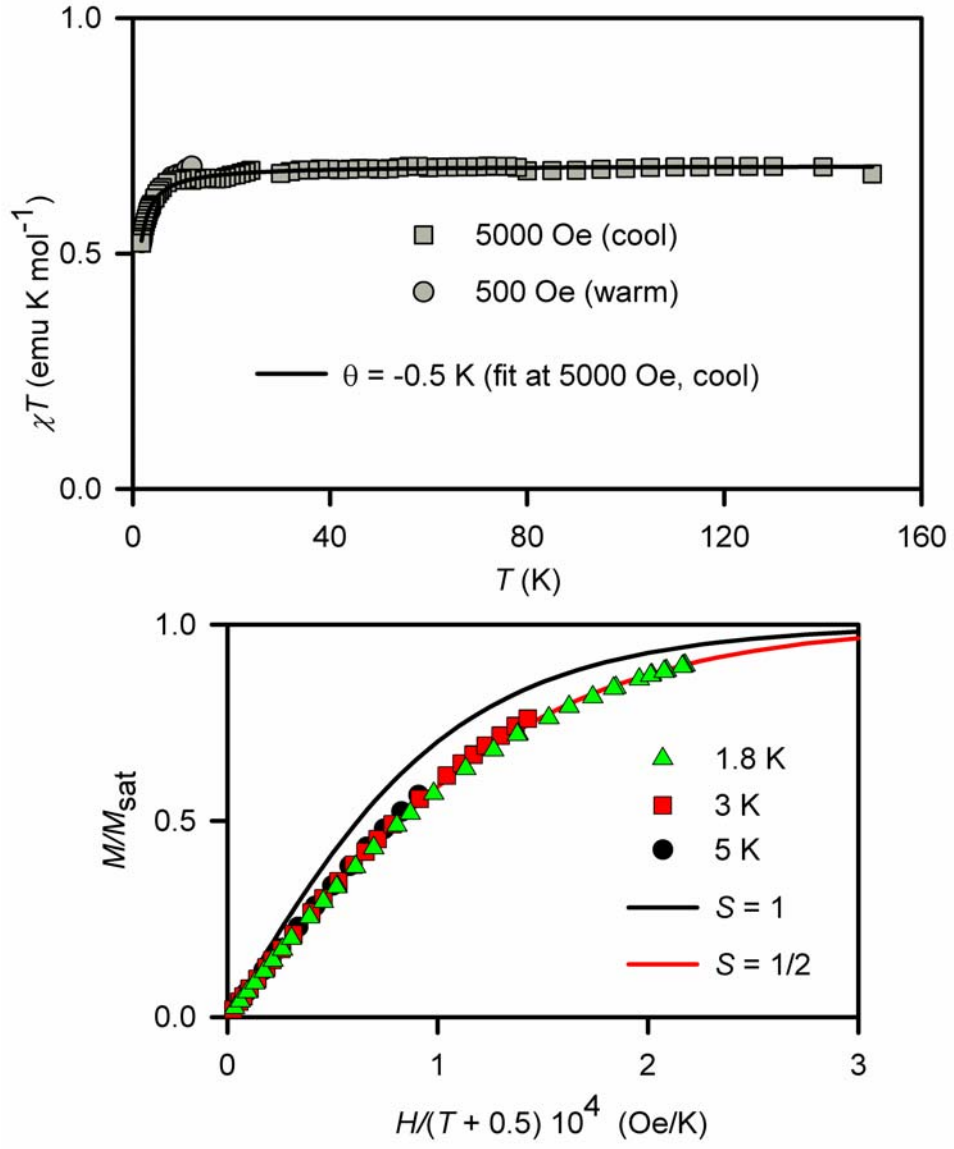

Figure S14. SQUID magnetometry for concentrated (24 mM) solution of nitroxide diradical **2** in THF (label: KD1247G). In the χT vs. T plots, the solid line corresponds to numerical fit to the Brillouin function of two independent spins $S = ½$ with the following variable parameters (parameter dependence and R^2): mean-field parameter, $\theta = –0.5$ K, and weight factor, $w = 0.91$ (0.35 and $R^2 = 0.999$). In the M/M_{sat} vs. $H/(T – \theta)$ plots at 1.8, 3, and 5 K, where $\theta = –0.5$ K is the mean-field parameter, the solid lines correspond to Brillouin functions with $S = ½$ and $S = 1$.

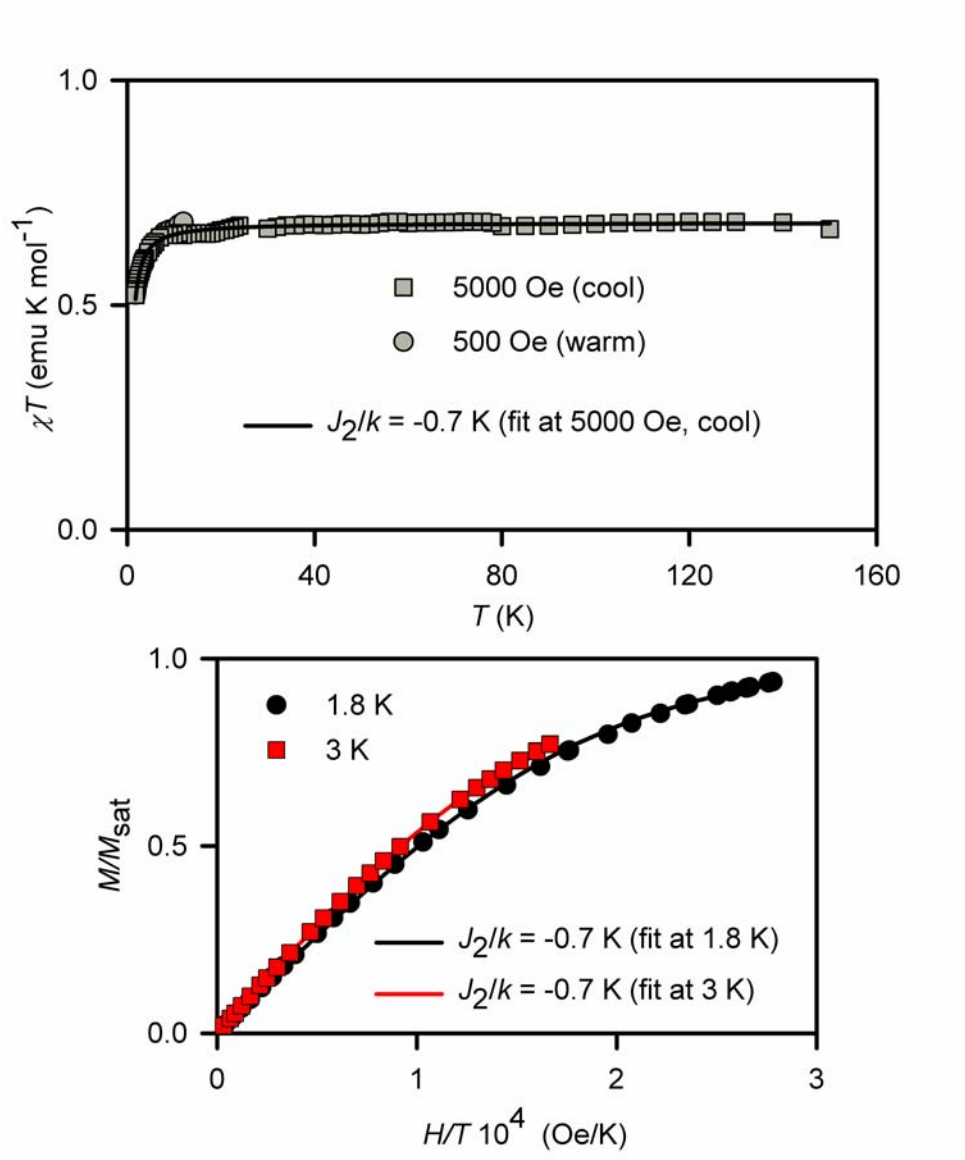

Figure S15. SQUID magnetometry for concentrated (24 mM) solution of nitroxide diradical **2** in THF (label: KD1247H) with numerical fits to the diradical model (eq. 4 with $J_1/k = 0$). The experimental data are identical to that in Figure S14. For the χT vs. T fits (top) and the M/M_{sat} vs. H/T fits (bottom), the variable parameters (parameter dependence and R^2) are as follows: at 5000 Oe in the cooling mode, $J_2/k = -0.7$ K, $w = 0.91$ (0.26, 0.990); at 1.8 K, $J_2/k = -0.7$ K, $M_{sat} = 0.85$ μ_B (0.63, 1.000); at 3 K, $J_2/k = -0.7$ K, $M_{sat} = 0.88$ μ_B (0.92, 1.000).

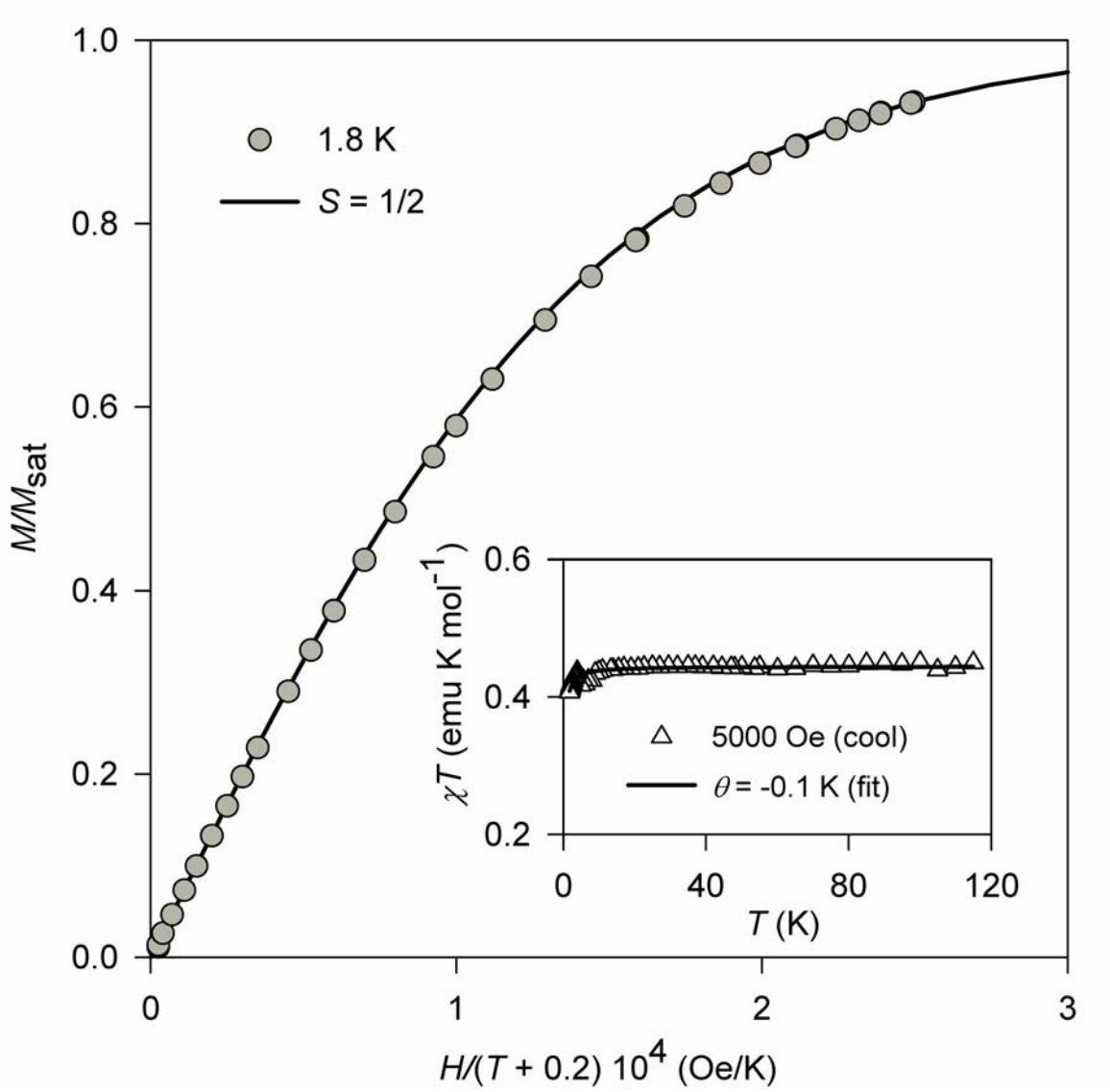

Figure S16. SQUID magnetometry for ~5 mM nitroxide diradical **2** in chloroform/methanol (1:1) (label: H0235r1G). Main plot: M/M_{sat} vs. $H/(T - \theta)$ at 1.8 K, where θ = –0.2 K is the mean-field parameter; the solid line corresponds to Brillouin function with S = ½. Inset plot: χT vs. T in cooling mode; the solid line corresponds to Brillouin function with S = ½ and mean-field parameter θ = –0.1 K.

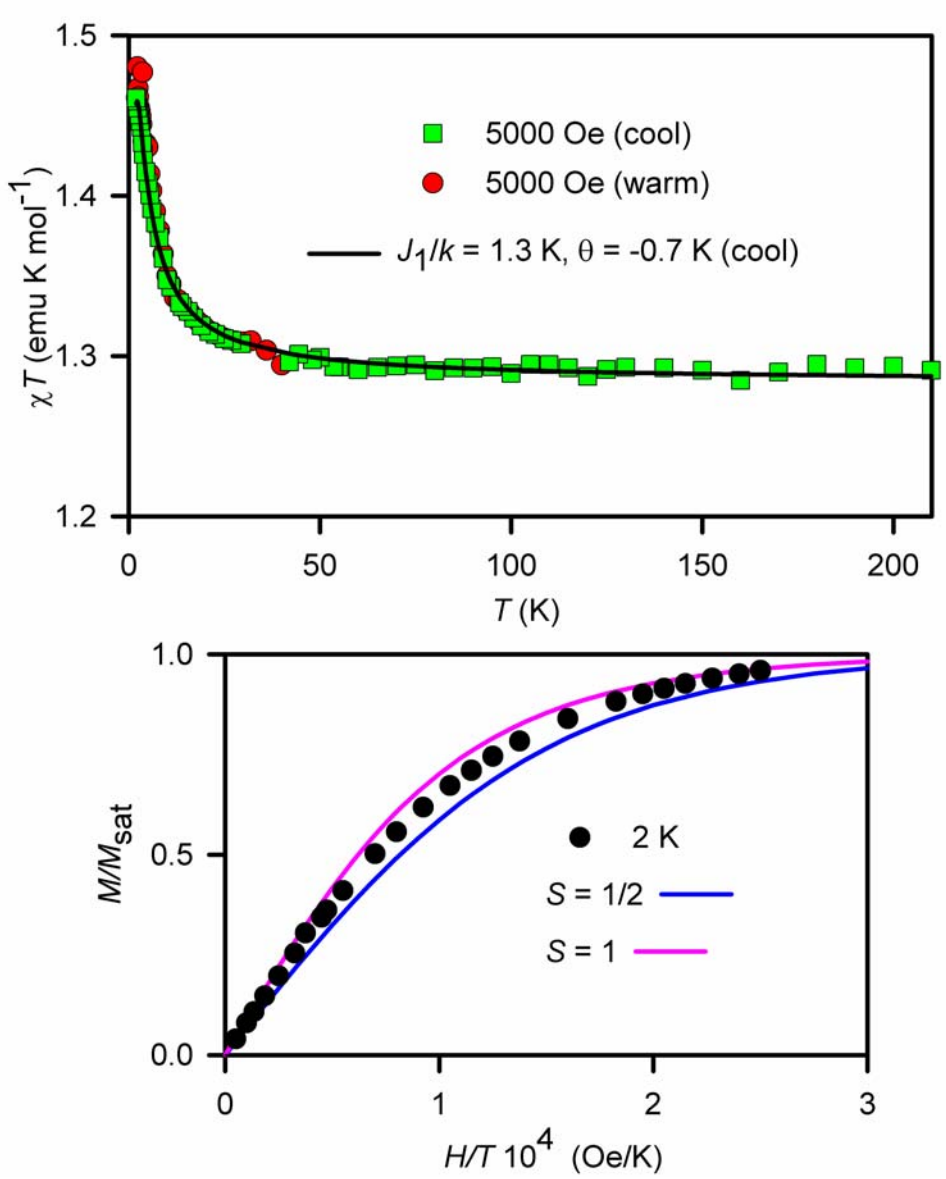

Figure S17. SQUID magnetometry for 20 mM **3** in 2-MeTHF (label: J1829RI) with numerical fit to the tetraradical model with mean-field parameter (Figure 10). The experimental data are identical to that in Figure 11 (main text). For the χT vs. T plot (top), the variable parameters (parameter dependence) for numerical at 5000 Oe in the warming mode are as follows: J_1/k = +1.3 K (0.98), θ = –0.7 K (0.98), w = 0.85 (0.56); R^2 = 0.997. For the M/M_{sat} vs. H/T plot at T = 2 K (bottom), theoretical Brillouin curves for paramagnet with S = ½ and S = 1 are shown.

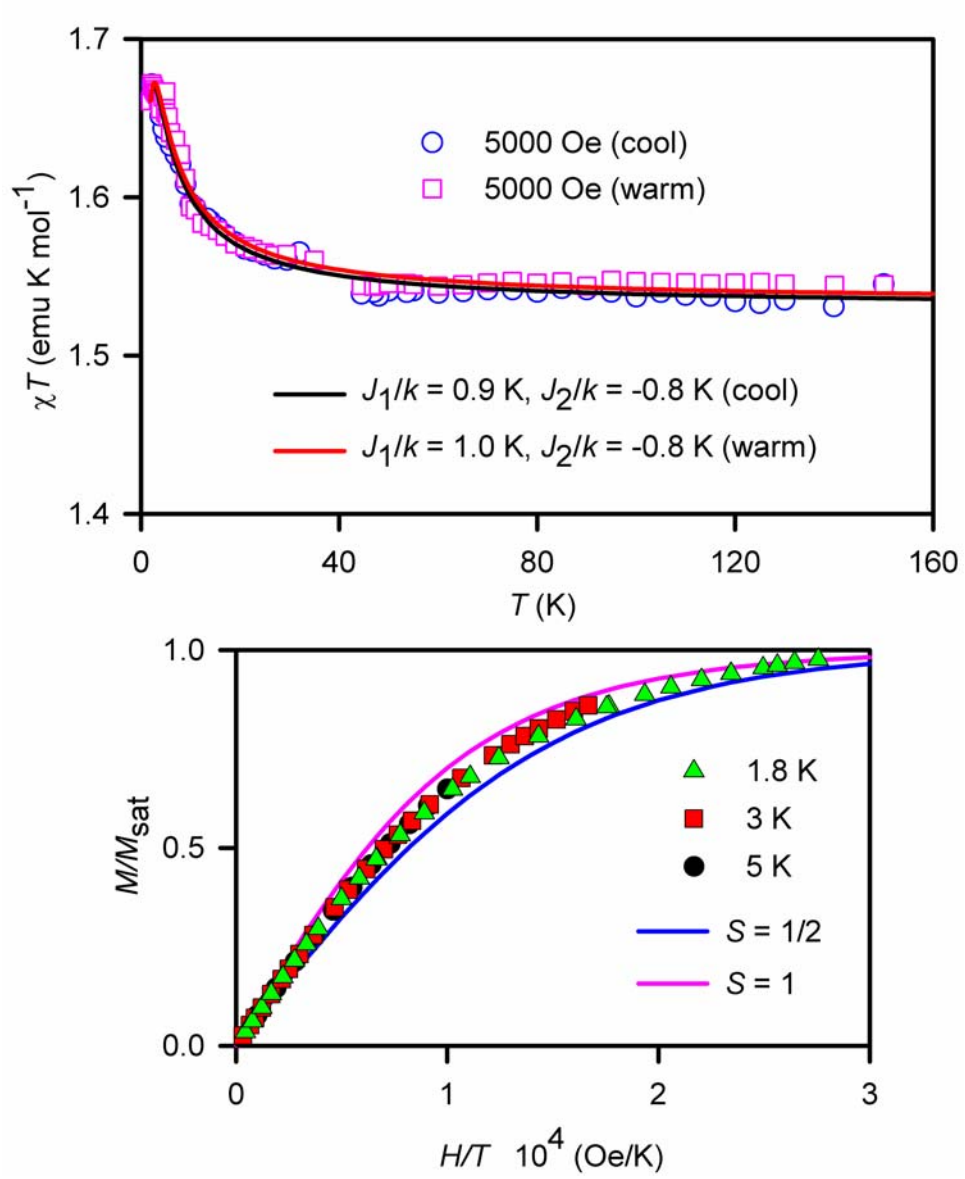

Figure S18. SQUID magnetometry for 15 mM **3** in THF (label: TR4081F3) with numerical fit to the tetraradical model (Figure 10, equation 2). For the χT vs. T plot (top), the variable parameters (parameter dependence) for the numerical fit to tetraradical model at 5000 Oe in the cooling mode are as follows: J_1/k = +0.9 K (0.98), J_2/k = –0.8 K (0.98), w = 1.02 (0.64); R^2 = 0.991. Analogous fit is obtained at 5000 Oe in the warming mode (R^2 = 0.986). For the M/M_{sat} vs. H/T plot at T = 2 K (bottom), theoretical Brillouin curves for paramagnet with S = ½ and S = 1 are shown.

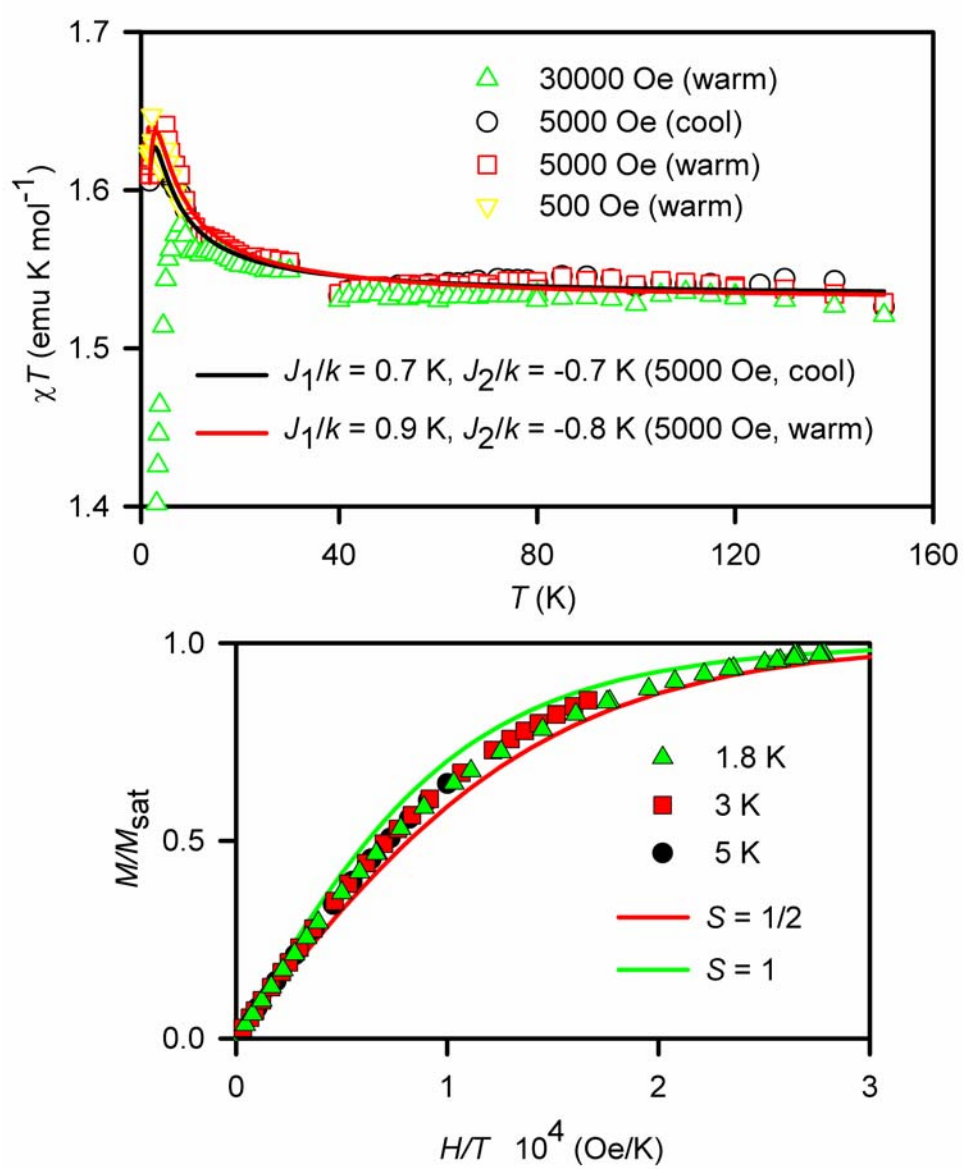

Figure S19. SQUID magnetometry for 15 mM **3** in THF (label: TR4081F6) with numerical fit to the tetraradical model (Figure 10, equation 2). For the χT vs. T plot (top), the variable parameters (parameter dependence) for the numerical fit to tetraradical model at 5000 Oe in the cooling mode are as follows: J_1/k = +0.7 K (0.98), J_2/k = –0.7 K (0.98), w = 1.02 (0.63); R^2 = 0.983. Analogous fit is obtained at 5000 Oe in the warming mode (R^2 = 0.978). For the M/M_{sat} vs. H/T plot at T = 2 K (bottom), theoretical Brillouin curves for paramagnet with S = ½ and S = 1 are shown.

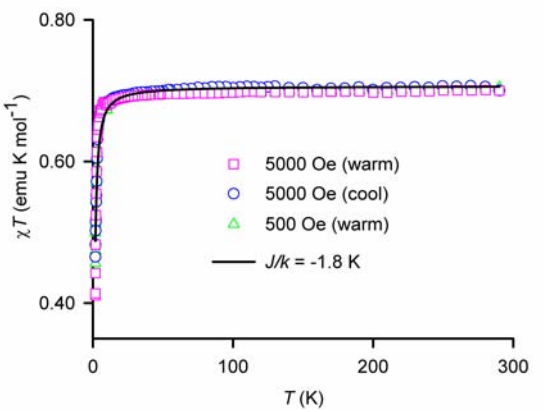

Figure S20. SQUID magnetometry for solid dinitroxide **2**: χT vs. T plots (label: H157R2H). The numerical fit (solid line) to the model of "diradical plus two S = ½ monoradicals" (eq. S5b) has the following variable parameters (and their parameter dependence) at 5000 Oe in the warming mode: J/k = –1.8 K and w = 0.94 (0.23).

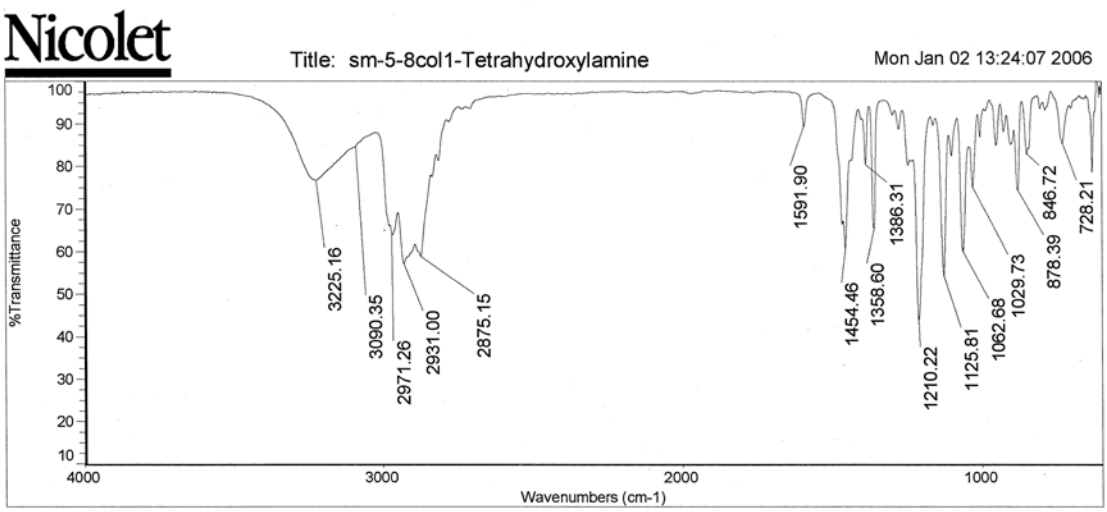

Number of sample scans: 128
Number of background scans: 128
Resolution: 4.000
Sample gain: 8.0
Mirror velocity: 0.6329
Aperture: 100.00

Figure S21. IR (ATR, ZnSe) spectrum of the calix[4]arene tetrahydroxylamine **5**.

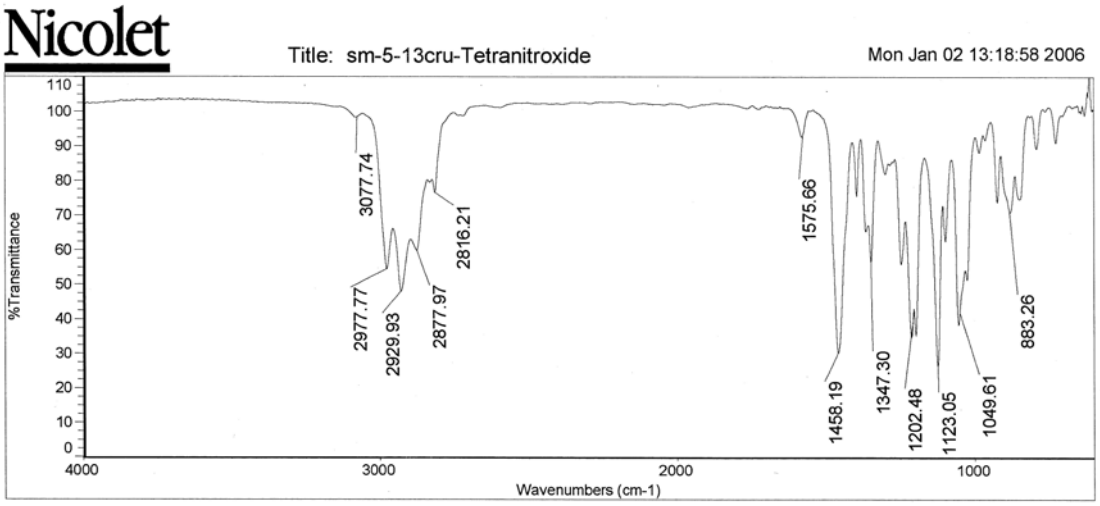

Number of sample scans: 128
Number of background scans: 128
Resolution: 4.000
Sample gain: 8.0
Mirror velocity: 0.6329
Aperture: 100.00

Figure S22. IR (ATR, ZnSe) spectrum of the calix[4]arene nitroxide tetraradical **1**.

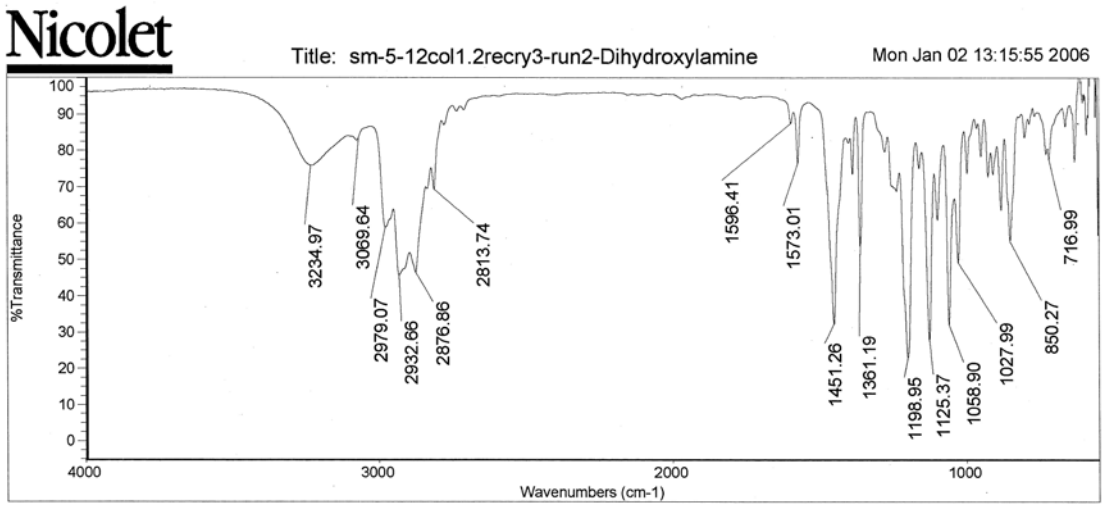

Figure S23. IR (ATR, ZnSe) spectrum of the calix[4]arene dihydroxylamine **6**.

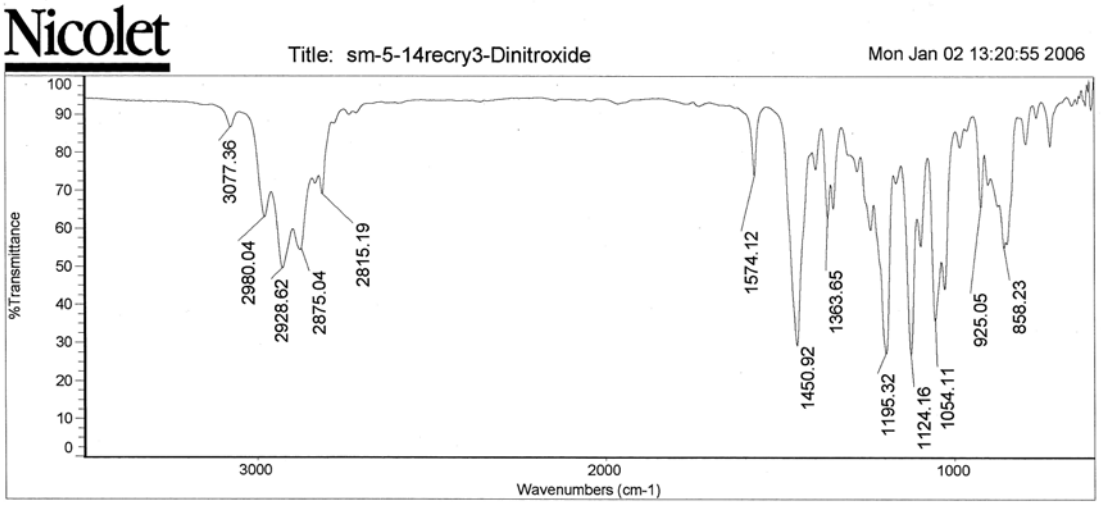

Figure S24. IR (ATR, ZnSe) spectrum of the calix[4]arene nitroxide diradical **2**.

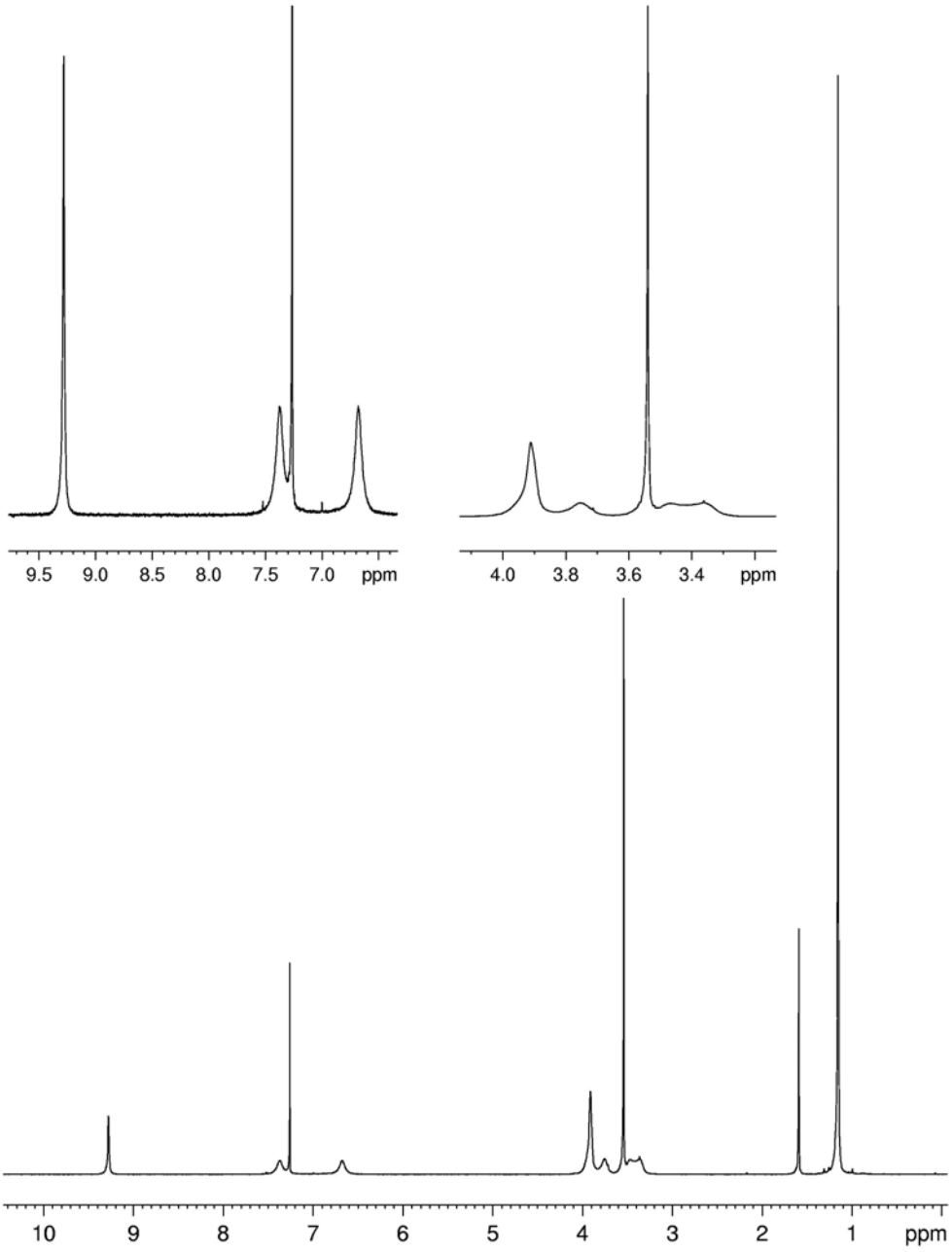

Figure S25. ^{1}H NMR (400 MHz, chloroform-*d*) spectrum of tetrahydroxylamine **5** (label: sm-10-17col1_run2).

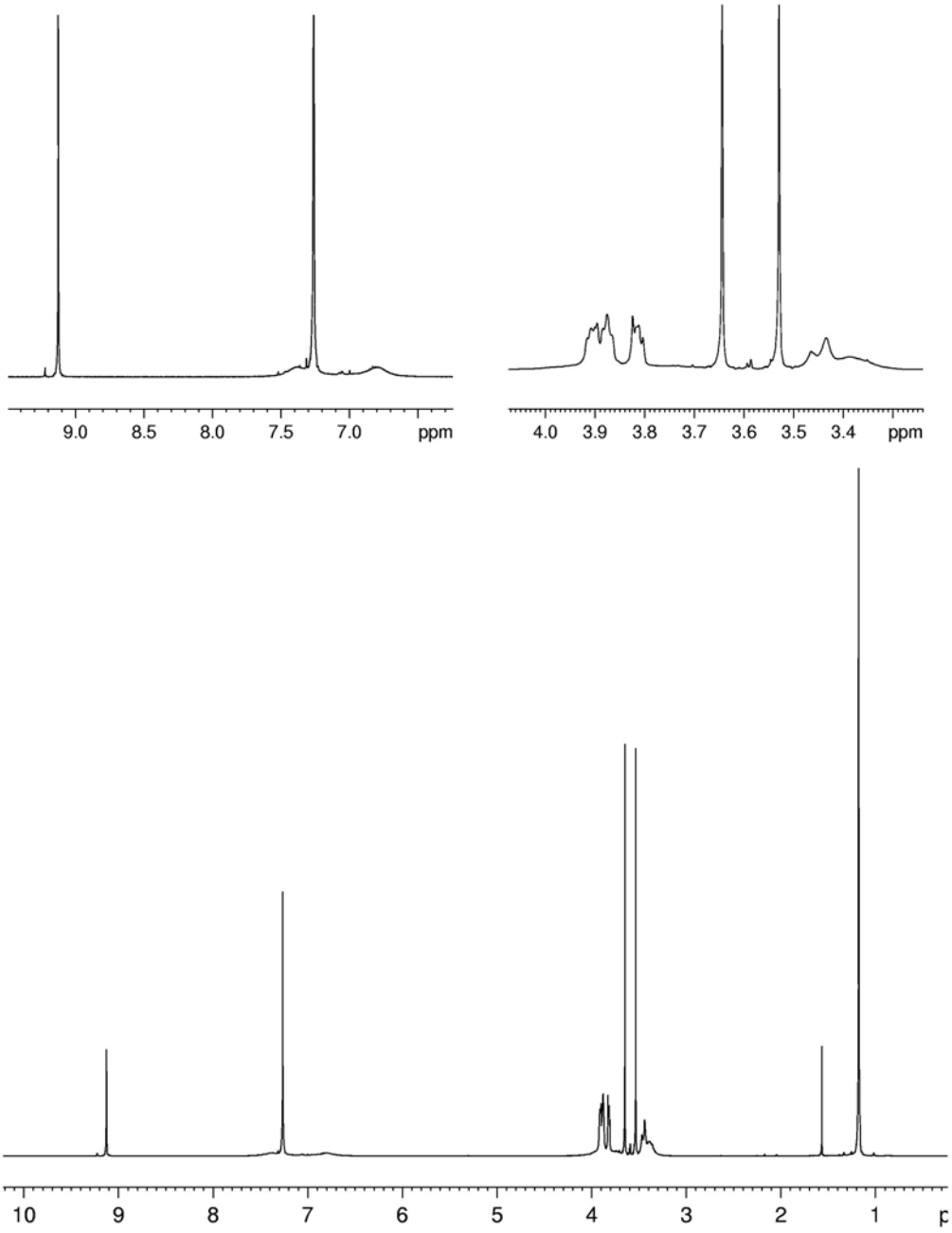

Figure S26. ^{1}H NMR (400 MHz, chloroform-*d*) spectrum of dihydroxylamine **6** (label: sm-10-11col1-run2).

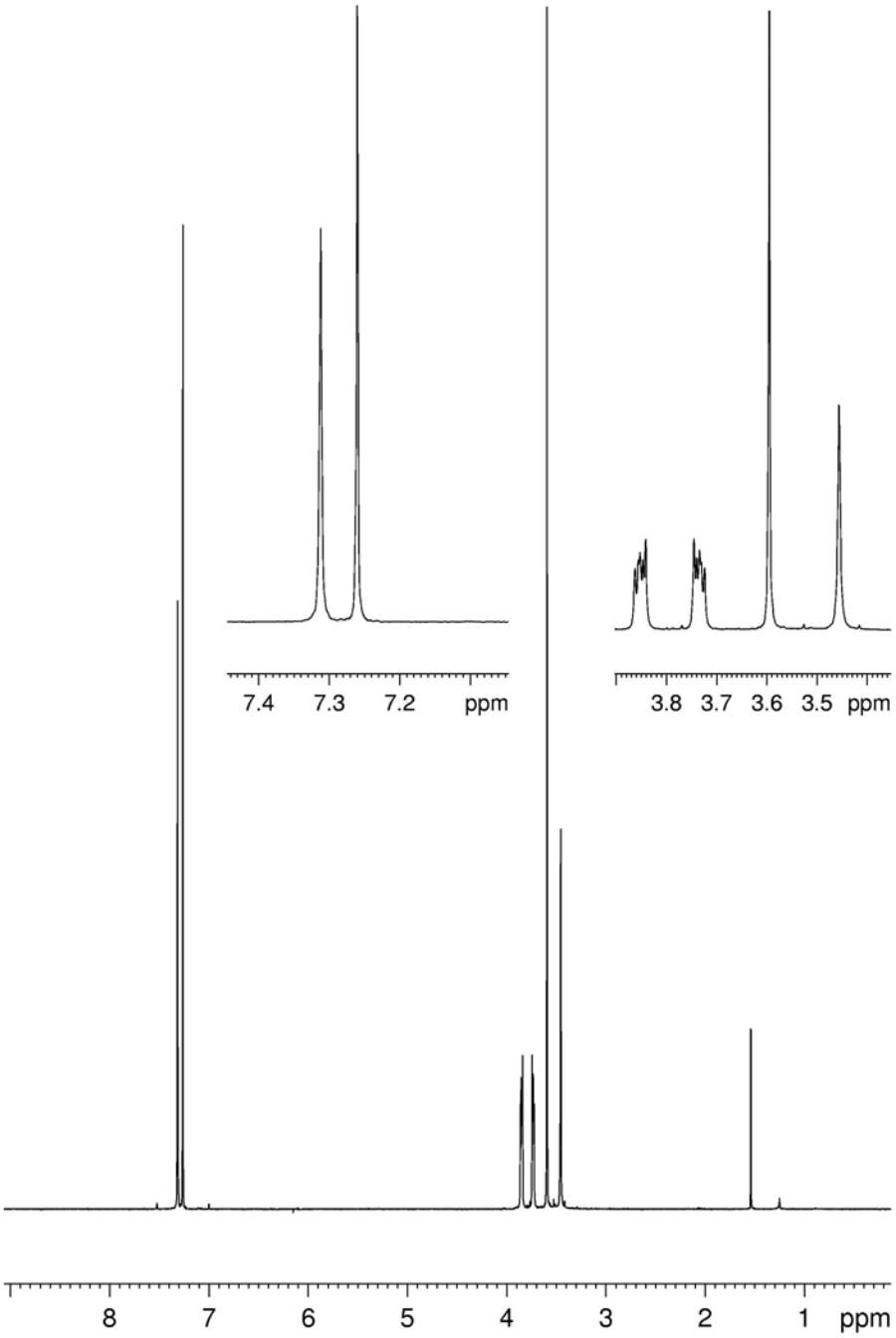

Figure S27. ^{1}H NMR (400 MHz, chloroform-*d*) spectrum of tetrabromocalix[4]arene **4** (label: SM-6-60recry1).